1   **Altered Hippocampal-Prefrontal Neural Dynamics in Mouse Models of Down Syndrome**

2

3   **Pishan Chang[1,2]**

4   **Daniel Bush[3]**

5   **Stephanie Schorge[1]**

6   **Mark Good[4]**

7   **Tara Canonica[4]**

8   **Nathanael Shing[1]**

9   **Suzanna Noy[2]**

10   **Frances K. Wiseman[2]**

11   **Neil Burgess[3]**

12   **Victor L.J. Tybulewicz[5, 6, 7]**

13   **Matthew C. Walker[1, 7, 8]**

14   **Elizabeth M.C. Fisher[2, 7]**

15   **1** Department of Clinical and Experimental Epilepsy, UCL Queen Square Institute of Neurology,
16   London, WC1N 3BG, UK

17   **2** Department of Neuromuscular Diseases, UCL Queen Square Institute of Neurology, London,
18   WC1N 3BG, UK

19   **3** UCL Institute of Cognitive Neuroscience, UCL Queen Square Institute of Neurology,
20   University College London, WC1N 3AZ, UK

21   **4** School of Psychology (College of Biomedical and Life Sciences), Cardiff University, Cardiff,
22   CF10 3AT, UK

23   **5** Francis Crick Institute, London, NW1 1AT, UK

24   **6** Department of Medicine, Imperial College, London, W12 0NN, UK

25   **7** These authors contributed equally

26   **8** Correspondence: m.walker@ucl.ac.uk

27

28   **Summary**

29   Altered neural dynamics in medial prefrontal cortex (mPFC) and hippocampus may contribute
30   to cognitive impairments in the complex chromosomal disorder, Down Syndrome (DS). Here,
31   we demonstrate non-overlapping behavioural differences associated with distinct
32   abnormalities in hippocampal and mPFC electrophysiology during a canonical spatial memory
33   task in three partially trisomic mouse models of DS (Dp1Tyb, Dp10Yey, Dp17Yey) that
34   together cover all regions of homology with human chromosome 21 (Hsa21). Dp1Tyb mice
35   showed slower decision-making (unrelated to the gene dose of *DYRK1A*, which has been
36   implicated in DS cognitive dysfunction) and altered theta dynamics (reduced frequency,
37   increased hippocampal-mPFC coherence, increased modulation of hippocampal high
38   gamma); Dp10Yey mice showed impaired alternation performance and reduced theta
39   modulation of hippocampal low gamma; while Dp17Yey mice were no different from wildtype
40   mice. These results link specific hippocampal and mPFC circuit dysfunctions to cognitive
41   deficits in DS models and, importantly, map them to discrete regions of Hsa21.

42

2

Introduction

Down syndrome (DS) is a complex cognitive disorder arising from trisomy of human chromosome 21 (Hsa21) with an incidence of ~1 in 800 live births worldwide [1]. The current global population of people with DS is estimated at 6 million [2] and prevalence is rising, primarily due to an increase in maternal age (a major risk factor for DS) and increased life expectancy in people with DS resulting from reduced infant mortality rates and improved access to healthcare [3–5]. DS is characterised by intellectual disability [6,7] and prominent impairments in planning, decision-making, and memory function [7–12] which likely arise from functional abnormalities of hippocampus and medial prefrontal cortex (mPFC) [6,8,9,13–16]. Increased dosage of single genes in Hsa21, such as *DYRK1A,* have been proposed to account for many of the alterations in neural development and abnormal phenotypes associated with DS, and thus to be targets for therapy development [17].

Activity in the hippocampus and mPFC can be characterised by oscillations in the theta and gamma bands. Hippocampal theta oscillations are associated with translational movement [18,19] and mnemonic function [20–22] across species, and can modulate synaptic plasticity [23]. Moreover, hippocampal theta modulates the amplitude of concomitant gamma oscillations both locally and across the neocortex [24–26], and task-related increases in phase-amplitude coupling are associated with successful memory encoding [27]. In humans, theta oscillations in mPFC are observed during working memory maintenance [28,29] and long-term memory retrieval [30,31], while increases in theta coherence between hippocampus and mPFC are associated with planning and decision-making across species [32–36].

To further elucidate the neural mechanisms underlying cognitive deficits associated with DS, we studied three chromosome engineered mouse models that each exhibit trisomy for one region of orthology with human chromosome Hsa21 – referred to here as the Dp1Tyb, Dp10Yey and Dp17Yey strains (full nomenclature given in Materials and Methods) [37,38]. In combination, these three mouse strains are triplicated for almost all the genes on Hsa21. We hypothesised that these trisomic mice might exhibit distinct cognitive impairments, corresponding to distinct alterations in oscillatory activity patterns within hippocampus and mPFC [15,16]. Hence, we carried out simultaneous local field potential (LFP) recordings from those regions while mice performed a canonical spatial alternation task which, importantly, can dissociate mnemonic function (i.e. alternation success) [39–41] from planning and decision-making processes (i.e. trial latency) [42–45].

Here, we demonstrate that distinct behavioural impairments associated with DS are exhibited by animals with different regions of homology and, crucially, that these impairments are associated with distinct alterations in neural dynamics across hippocampus and mPFC. Moreover, reducing the 'dose' of *Dyrk1a* – a gene which has been suggested to be critically important for neural function in DS [46–51] - was not sufficient to rescue the observed differences in behaviour, supporting the concept that cognitive impairments in DS do not necessarily map to single genes. By taking an unbiased approach to the gene content of these partially trisomic mice, and by combining behavioural and electrophysiological methodologies, we have therefore identified critical circuit dysfunction in DS models that paves the way for future determination of key dosage-sensitive gene combinations underlying cognitive phenotypes in this complex chromosomal disorder.

88   **Results**

89   **Impaired Spatial Memory in Dp10Yey Mice and Decision-Making in Dp1Tyb Mice**

90   Impairments in planning, decision making, and memory function have a significant impact on
91   the lives of people with DS. In order to dissect the mechanisms underlying these cognitive
92   deficits, we studied three mouse lines that are triplicated for the three mouse chromosome
93   regions syntenic to Hsa21. The Dp1Tyb mouse strain has a 23Mb duplication of the Hsa21-
94   syntenic region of Mmu16 which contains 148 coding genes with orthologues on Hsa21 [37];
95   the Dp10Yey strain is duplicated for the Hsa21-syntenic region of Mmu10, which encodes 39
96   Hsa21 protein coding genes; and the Dp17Yey line is duplicated for the Hsa21-syntenic region
97   of Mmu17 which encodes 19 protein coding genes [38]. Together, these mice make up a
98   'mapping panel', such that phenotypes found in any one strain are likely to arise from having
99   an additional (i.e. third) copy of the specific Hsa21 orthologues within that strain.

100   We began by comparing cognitive function in male Dp1Tyb, Dp17Yey and Dp10Yey mice at 3
101   months of age with age- and sex- matched WT littermate control cohorts using a canonical
102   spatial alternation task (Figure 1a-c; see Supplementary Figure 1a,b for further details and
103   Supplementary Table 1 for trial and animal numbers). Importantly, this task can assay both
104   mnemonic function (by examining the propensity to spontaneously alternate between goal
105   arms on successive trials) and decision making (by examining the time taken to choose and
106   enter a goal arm). Intriguingly, we found that distinct functional deficits were exhibited by
107   each mutant mouse strain, suggesting that trisomy of discrete Hsa21 orthologues can have
108   divergent effects on cognitive function.

109   First, we found that Dp10Yey mice exhibited alternation rates that were significantly lower
110   than their WT littermates and did not differ from chance (Figure 1e). In contrast, alternation
111   rates in Dp1Tyb and Dp17Yey mice did not differ from those of WT mice and were significantly
112   above chance in both strains (Figure 1d,f), with no difference in alternation rates between WT
113   cohorts (Supplementary Figure 2a). These results suggest that Dp10Yey mice have impaired
114   memory function, while Dp1Tyb and Dp17Yey mice are spared.

115   Second, we examined trial latencies, defined as the time taken to make a final crossing of the
116   decision point prior to turning into the goal arm (see Materials and Methods). We found that
117   these were significantly greater in Dp1Tyb mice compared to their WT littermates (Figure 1g);
118   while no differences were observed between Dp10Yey or Dp17Yey mice and their respective
119   control groups (Figure 1h,i) or between any of the WT cohorts (Supplementary Figure 2b).
120   Importantly, the increased trial latency exhibited by Dp1Tyb mice could not simply be
121   accounted for by motor impairments, independent of decision making processes, as we found
122   no differences in average running speed between any mutant mouse group and their WT
123   littermates. Conversely, Dp1Tyb mice spent a significantly greater proportion of each trial
124   immobile, prior to making a decision, with no differences between either of the other mutant
125   mouse strains and their control groups (Supplementary Figure 3). In sum, these results
126   suggest that decision-making processes are disrupted in Dp1Tyb mice, despite relatively intact
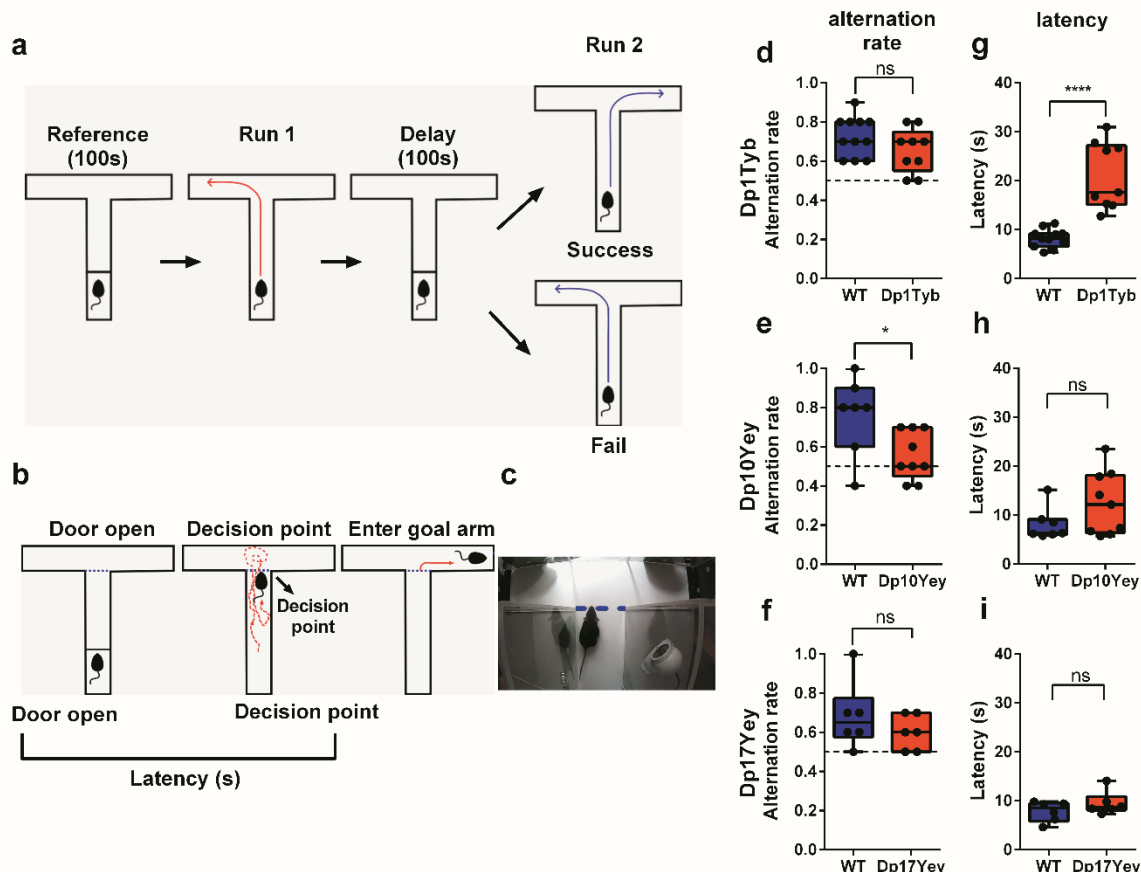127   mnemonic function, while Dp10Yey and Dp17Yey mice are spared.

Figure 1: Spatial Alternation Rate and Trial Latency in Mouse Models of DS

(a) Schematic experimental procedure (see Supplementary Figure 1a,b for further details). **(b)** Schematic method for computing trial latency: the time between raising the door to release the animal from the start area, to the point at which the mouse's nose crosses the 'decision point' (blue dashed line) before entering a goal arm. **(c)** Example of one animal reaching the decision point. **(d-f)** Alternation rate and **(g-i)** trial latency for each DS mouse model compared to their wild-type (WT) control group, showing: (e) significant differences in alternation rate for Dp10Yey vs WT mice (t(14)=2.48, p<0.05); and (g) significant differences in trial latency for Dp1Tyb vs WT mice (t(18)=5.97, p<0.001); but no differences in either measure for Dp17Yey vs WT mice. Chance alternation rate is shown as a black dotted line. Data are presented as box-whisker plots indicating the median, 25th and 75th percentiles, minimum and maximum values, with data for individual mice superimposed. Please refer to Supplementary Table 1 for trial and animal numbers, and Supplementary Table 2 for full details of all statistical analyses.

Finally, previous studies of transgenic mouse models of DS have led to the proposal that the overexpression of *Dyrk1a* (and thus an increased dosage of the DYRK1A protein) makes a critical contribution to neurological and behavioural abnormalities by shifting the excitation/inhibition balance towards inhibition, for example [16,52]. The *Dyrk1a* gene maps to the Mmu16 region of Hsa21 and so is duplicated within the Dp1Tyb strain. To assess the behavioural consequences of altering the copy number of *Dyrk1a* in Dp1Tyb mice, we crossed Dp1Tyb animals with mice carrying a disrupted *Dyrk1a* gene to generate Dp1Tyb*Dyrk1aKO mice that are still duplicated for 147 Hsa21-orthologous coding genes on Mmu16, but have

151   only 2 functional copies of *Dyrk1a*. Interestingly, these Dp1Tyb*Dyrk1aKO mice exhibited
152   both a similar alternation rate to Dp1Tyb mice and a similarly prolonged decision-making
153   (latency) phenotype (Supplementary Figure 4). Thus, reduction of the *Dyrk1a* copy number
154   from three to two did not rescue the increased trial latency exhibited by Dp1Tyb mice. This
155   finding indicates that triplication of *Dyrk1a* is not necessary to produce the decision-making
156   deficit in Dp1Tyb mice, which must therefore arise from other gene(s) in this region of Hsa21
157   homology.

158

Reduced Theta Frequency in Dp1Tyb Mice

160   Successful memory encoding and retrieval are associated with increased theta power in both
161   hippocampus [20–22] and mPFC [28–31] across species. Furthermore, a reduction in hippocampal
162   theta frequency has been directly linked to impaired spatial memory performance in a rodent
163   model of temporal lobe epilepsy [53]. Hence, we next analysed LFP recordings from
164   hippocampus and mPFC during spatial alternation in the T-maze (see Supplementary Figure 5
165   for details of electrode placement). Initially, we focused our analyses on a 10s window
166   centred on the time at which animals crossed the decision point, and which would incorporate
167   periods of memory encoding and retrieval from the sample and choice runs, respectively (see
168   Materials and Methods for further details).

169   As expected, average power spectra from the mPFC (Figure 2a-c), and hippocampus (Figure
170   2d-f) across all animals showed a prominent peak in the 6-12Hz theta band during this period.
171   Interestingly, although theta power did not differ between mouse lines, we found that theta
172   frequency in both the mPFC (Figure 2a) and hippocampus (Figure 2d) was consistently lower
173   in Dp1Tyb mice compared to WT controls. In contrast, no difference in theta frequency was
174   observed in either region in Dp10Yey or Dp17Yey mice compared to their control cohorts
175   (Figure 2b,c,e,f), or between WT cohorts (Supplementary Figure 2c,d).

176   To establish whether the reduction in theta frequency observed in Dp1Tyb mice arose simply
177   from the increased time that those animals spent immobile, we subsequently restricted our
178   analysis to periods of movement only (see Materials and Methods). Consistent with the
179   results above, theta frequency in both the hippocampus and mPFC of Dp1Tyb mice was still
180   significantly lower than WT controls when periods of immobility were excluded. Moreover,
181   this resulted from a reduction in the intercept, but not the slope, of the running speed v theta
182   frequency relationship in both regions (Supplementary Figure 6a-d). In sum, these data
183   suggest that Dp1Tyb mice, which exhibit slower decision making, also show a general slowing
184   of theta band oscillations across hippocampal and medial prefrontal regions during spatial
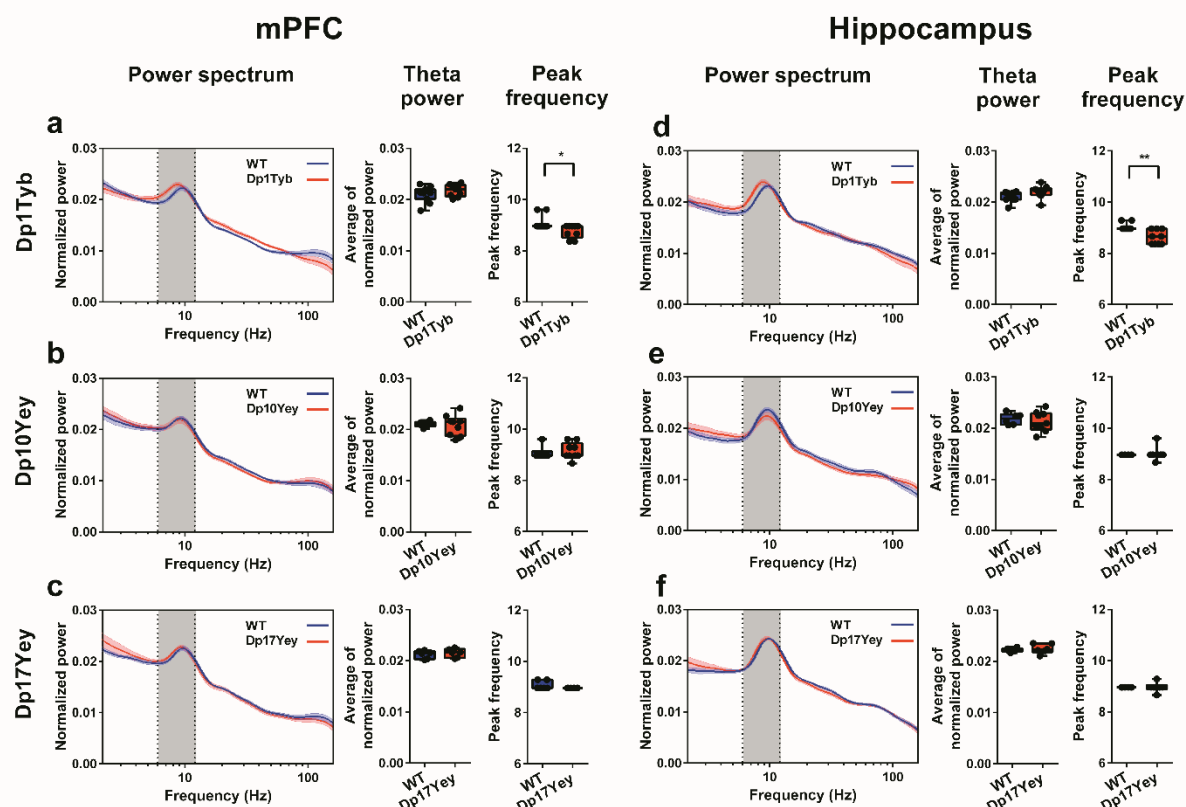185   alternation, independent of running speed.

Figure 2: Theta Oscillations in mPFC and Hippocampus during Spontaneous Alternation

Power spectra, mean theta power and peak theta frequency in **(a-c)** mPFC and **(d-f)** hippocampus for **(a, d)** Dp1Tyb and WT; **(b, e)** Dp10Yey and WT; **(c, f)** Dp17Yey and WT animals during spontaneous alternation in the T-maze. Grey rectangles indicate the 6-12Hz theta band. There are no differences in theta power between mutant mice and WT groups in either mPFC or hippocampus. However, peak theta frequency in Dp1Tyb animals is significantly lower than WT in both: **(a)** mPFC (Dp1Tyb: 8.76±0.26Hz; WT: 9.08±0.26Hz; Mann–Whitney U=22.5, p<0.05); and **(d)** hippocampus (Dp1Tyb: 8.63±0.28Hz; WT: 9.02±0.13Hz; Mann–Whitney U=13.5, p<0.005), but no different in the other mutant mouse groups compared to their control populations (Mann–Whitney U test, all p>0.4). Data are presented as box-whisker plots indicating the median, 25th and 75th percentiles, minimum and maximum values, with data for individual mice superimposed. Please refer to Supplementary Table 2 for full details of all statistical analyses.

7

Altered Hippocampal Phase-Amplitude Coupling in Dp1Tyb and Dp10Yey Mice

Coherence between the phase of theta oscillations and the amplitude of concurrent gamma band oscillations is prevalent in the rodent hippocampus [54,55] and across human neocortex [25]. In addition, theta-gamma phase-amplitude coupling (PAC) has been implicated in successful memory function [27,56]. Hence, we asked whether the three DS mouse lines exhibited abnormal PAC that might be associated with the observed differences in behaviour. Average cross-frequency coherence images across all animals revealed two distinct PAC peaks in the hippocampal LFP: one between 6-12Hz theta and 60-120Hz 'low gamma' (LG) oscillations; and another between 6-12Hz theta and 140-160Hz 'high gamma' (HG) oscillations (Supplementary Figure 7a), while theta phase modulation of LG or HG amplitude was entirely absent in mPFC (Supplementary Figure 7b).

Interestingly, subsequent analyses indicated that the magnitude of hippocampal PAC in each pair of frequency bands also differed between specific DS models and WT controls. First, we found that theta-HG PAC was significantly increased in the Dp1Tyb group – which exhibited slowed decision making - relative to WT controls, but not in any other mouse strain (Figure 3a). Secondly, we found that theta-LG PAC was significantly reduced in the Dp10Yey group – which showed impaired spatial alternation - relative to WT controls, but not in any other strain (Figure 3b). Importantly, there was no alteration in hippocampal PAC across any pair of frequency bands in Dp17Yey animals, which also exhibit no differences in behaviour compared to their WT control group (Figure 3c), and no differences in theta-LG or theta-HG PAC between WT cohorts (Supplementary Figure 2e, f). In addition, we found no evidence for a difference in LG or HG power between mutant mice and their WT controls (Supplementary Figure 8).

To confirm that the increased theta-HG PAC observed in Dp1Tyb mice did not arise from the observed differences in movement statistics, we subsequently removed any effect of average time spent immobile on average theta-HG PAC values across animals in both mutant and control groups by linear regression, and then compared the residual values between groups. This analysis confirmed that the increased theta-HG PAC in hippocampus exhibited by Dp1Tyb mice was independent of differences in movement statistics (Supplementary Figure 6e,f). In sum, these data distinguish changes in hippocampal theta phase modulation of local high (Dp1Tyb) and low (Dp10Yey) gamma amplitude in a manner that can be associated with increased trial latency and impaired spatial alternation, respectively.
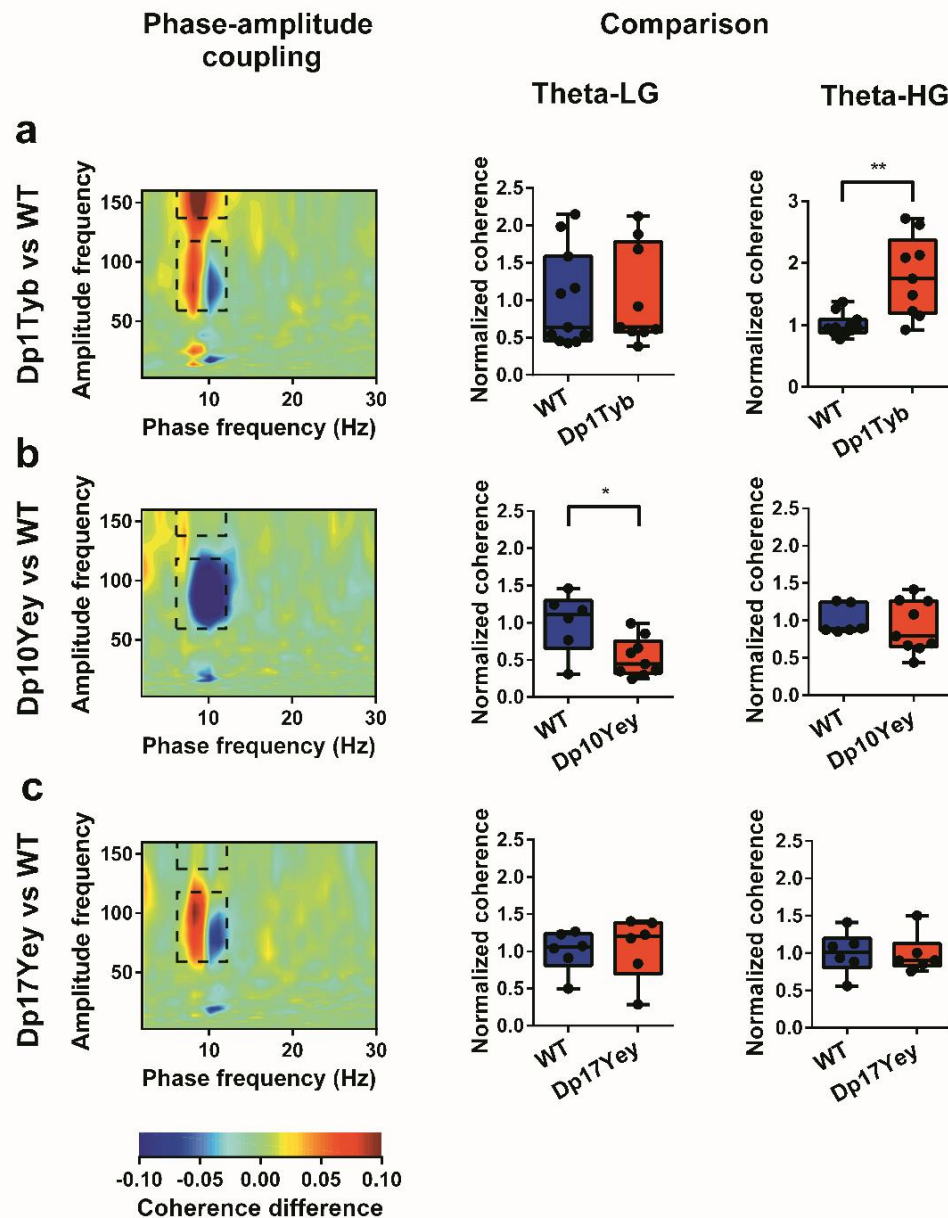
8

231

Figure 3: Hippocampal Phase-amplitude Coupling during Spontaneous Alternation

(a-c) Left: Comodulograms showing differences in hippocampal phase-amplitude coupling between each mutant mouse group and WT, with warm colours indicating stronger coupling in DS mice. These illustrate two prominent peaks – one between 6-12Hz theta phase and 60-120Hz 'low gamma' (LG) amplitude, and another between 6-12Hz theta phase and 140-160Hz 'high gamma' (HG) amplitude (black dashed rectangles; see Supplementary Figure 7 for further details). Right: Theta-LG and theta-HG cross-frequency coherence values, normalized by the mean value in the corresponding WT control cohort to facilitate comparison. **(a)** Dp1Tyb mice show no difference in theta-LG coupling, but significantly greater theta-HG coupling, compared to WT (Mann–Whitney U=11.0, p<0.01). **(b)** Conversely, Dp10Yey mice show significantly lower theta-LG coupling (Mann–Whitney U=8.0, p<0.05), but no difference in theta-HG coupling, compared to WT. **(c)** Finally, Dp17Yey mice show no difference in either theta-LG or theta-HG compared to WT. Data are presented as box-whisker plots indicating the median, 25th and 75th percentiles, minimum and maximum values, with data for individual mice superimposed. Please refer to Supplementary Table 2 for full details of all statistical analyses.

9

Increased Hippocampal-mPFC Theta Coherence in Dp1Tyb Mice

Planning, decision-making, memory encoding and retrieval processes are each associated with increased functional connectivity between the hippocampus and mPFC in both rodents [32–34,57] and humans [31,36]. Interestingly, abnormalities in functional connectivity have also been implicated in various neurodevelopmental disorders, including DS [15,58]. Hence, we next examined theta and gamma band coherence between hippocampus and mPFC, with the hypothesis that differences in functional connectivity between those regions might be associated with the cognitive impairments observed in these DS mice.

First, we found that theta coherence between the hippocampus and mPFC was significantly greater in Dp1Tyb mice compared to WT littermates (Figure 4a), while no such differences were observed between Dp10Yey or Dp17Yey mice and their control groups (Figure 4b,c), or between WT cohorts (Supplementary Figure 2g). In addition, there were no differences in either low or high gamma coherence between hippocampus and mPFC in any mutant mouse group compared to their WT controls (Supplementary Figure 9). To confirm that the increased theta coherence observed in Dp1Tyb mice, compared to their WT littermates, did not simply arise due to the observed differences in movement statistics, we again removed any effect of average time spent immobile on theta coherence values across animals in both groups by linear regression, and then compared the residual values between groups (Supplementary Figure 6g,h). This confirmed that the increased theta coherence exhibited by Dp1Tyb mice was independent of differences in movement statistics.

To further characterise potential changes in functional connectivity across mouse lines, we extracted the theta phase lag between hippocampus and mPFC in order to assess the direction of communication between these regions (Figure 4d-f). In each group of animals, we found that hippocampal theta oscillations led those in mPFC by ~1 radian, which is equivalent to ~20ms for a 6-12Hz theta oscillation, without any difference between strains. Intriguingly, these results indicate that Dp1Tyb mice – which exhibit slowed planning and decision-making behaviour during the spatial alternation task – showed increased theta-band coherence between hippocampus and mPFC, without any differences in the direction of communication between those regions. This suggests that cognitive dysfunction arising from these electrophysiological differences is due to an increased influence of hippocampal inputs on medial prefrontal dynamics, rather than changes in the direction of information flow between regions.
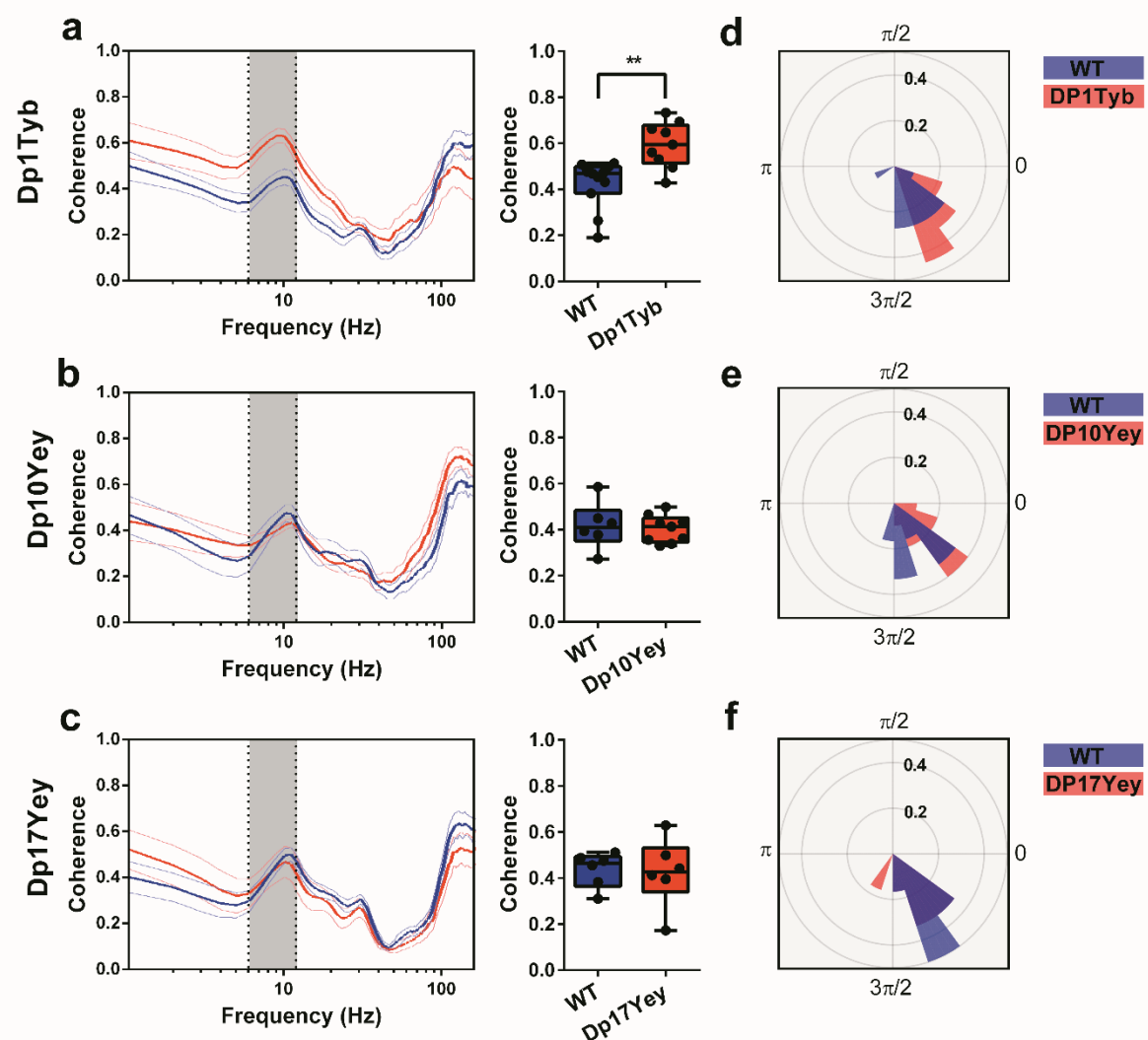
Figure 4: Hippocampal-medial prefrontal Phase Coupling during Spontaneous Alternation

(a-c) Coherence spectra and mean theta band coherence illustrating hippocampal-mPFC phase coupling during spontaneous alternation behaviour. Grey rectangles indicate the 6-12Hz theta band. **(a)** Theta band coherence is significantly greater in Dp1Tyb mice compared to WT (Mann-Whitney U=11.0, p<0.005), while there is no difference between either **(b)** Dp10Yey and WT or **(c)** Dp17Yey and WT animals. **(d-f)** Circular mean phase offset between mPFC and hippocampus for **(d)** Dp1Tyb and WT; **(e)** Dp10Yey and WT; and **(f)** Dp17yey and WT animals. The radial axis shows relative frequency, and the polar axis indicates the circular mean theta phase difference between mPFC and hippocampus. These results suggest that hippocampal theta oscillations lead those in mPFC by ~1 radian (equivalent to ~20ms at 9Hz) in all mutant and WT mice, without any differences between groups (Watson-Williams test, all p>0.07). Data are presented as box-whisker plots indicating the median, 25th and 75th percentiles, minimum and maximum values, with data for individual mice superimposed. Please refer to Supplementary Table 2 for full details of all statistical analyses.

Behavioural and LFP Characteristics are preserved across the Lifespan in DS Mouse Models

292

293   Finally, we asked whether the behavioural and LFP abnormalities observed in Dp1Tyb and
294   Dp10Yey mice persisted throughout life, or were specific to the adolescent period during
295   which they were initially tested [59]. To this end, we repeated tests of alternation behaviour
296   and recorded LFP data from the same animals at six and nine months of age, alongside age
297   matched WT controls (see Supplementary Figure 1c for further details, Supplementary Table
298   3 for animal and trial numbers). Importantly, we found that the differences in both behaviour
299   and neural dynamics described above remained stable throughout this long-term assessment
300   period.

301   First, we found that trial latency was significantly greater in Dp1Tyb mice compared to their
302   WT control group across all three time points (Figure 5a), and the observed reduction in both
303   hippocampal and mPFC peak theta frequency also persisted with age (Figure 5b,c). Similarly,
304   hippocampal theta-HG phase-amplitude coupling was significantly greater in Dp1Tyb mice
305   compared to WT at all ages (Figure 5d); and theta coherence between hippocampus and
306   mPFC remained significantly higher than WT across the lifespan (Figure 5e).

307   Second, we found that the impaired alternation rate observed in young Dp10Yey mice
308   persisted with age (Figure 5f). In contrast to WT mice, the alternation rate in Dp10Yey mice
309   was not different from chance at any time point. Similarly, hippocampal theta-LG phase-
310   amplitude coupling remained consistently lower in Dp10Yey mice relative to WT controls
311   (Figure 5g). In sum, these results suggest that the observed differences in behaviour and
312   neural dynamics between these DS mouse models and their WT control groups generally
313   remained stable throughout adulthood, suggesting that aging neither alleviated nor
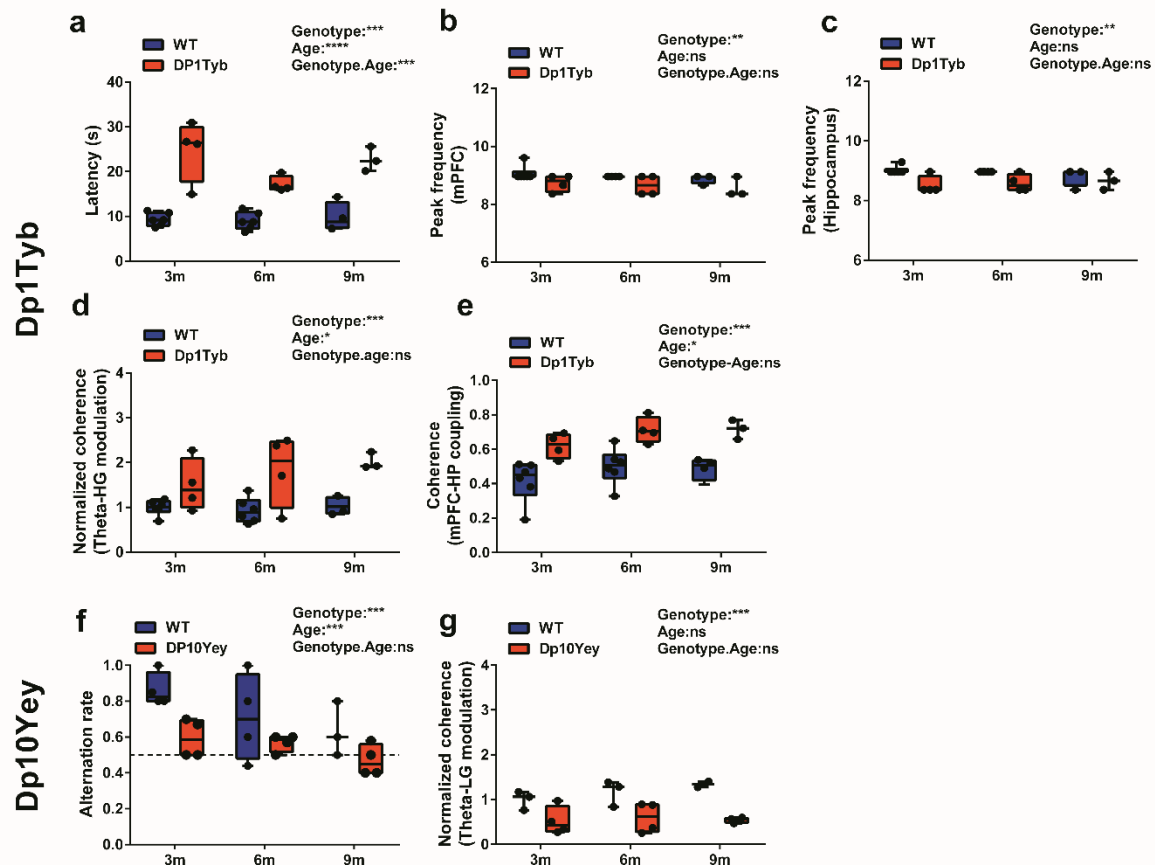314   worsened the phenotype in either strain.

12

Figure 5: Behavioural and Electrophysiological Data across the Lifespan

Behavioural and LFP data at 3-4months (3m), 6-7 months (6m) and 9-10 months (9m) of age in: **(a-e)** Dp1Tyb; and **(f,g)** Dp10Yey mice. **(a)** Trial latency remains significantly greater in Dp1Tyb mice compared to WT throughout the lifespan (GLM, Type III tests $\chi^2(1)=56.1$, p<0.0001). Similarly, peak theta frequency in both **(b)** mPFC (GLM, Type III $\chi^2(1)=6.84$, p<0.01) and **(c)** hippocampus (GLM, Type III $\chi^2(1)=8.93$, p<0.01) is shifted to a significantly lower frequency. **(d)** Hippocampal theta-HG phase-amplitude coupling (GLM, Type III $\chi^2(1)=14.2$, p<0.0001) and **(e)** theta coherence between mPFC and hippocampus (GLM, Type III $\chi^2(1)=29.6$, p<0.0001) are also increased in Dp1Tyb mice at all three time points, compared to their WT control group. **(f)** Alternation rate remains significantly lower in Dp10Yey mice compared to WT throughout the lifespan (GLM, Type III $\chi^2(1)=12.5$, p<0.0001), and does not differ from chance level (black dashed line) at any age (Friedman's test, $\chi^2(5)=8.2$, p>0.15), while the WT control group consistently perform above chance (Friedman's $\chi^2(5)=10.3$, p<0.05). **(g)** Hippocampal theta-LG phase-amplitude coupling is also significantly lower in Dp10Tyb mice at all three time points (GLM, Type III $\chi^2(1)=18.2$, p<0.0001). Data are presented as box-whisker plots indicating the median, 25th and 75th percentiles, minimum and maximum values, with data for individual mice superimposed. Please refer to Supplementary Table 2 for full details of all statistical analyses.

13

Discussion

The present study reveals distinct cognitive deficits and electrophysiological differences in three mouse models of DS which, combined, carry duplications covering all of the Hsa21-orthologous regions. By taking an unbiased approach, we aimed to discover if cognitive deficits resulting from triplication of genes/DNA elements in Hsa21 could be linked to individual regions with different sequence contents. As a measure of cognitive function, we used a canonical test of spatial memory - spontaneous alternation in a T-maze [60]. This behavioural test probes both decision-making and mnemonic function, based on the premise that mice have evolved an optimal strategy to explore their environment that relies on memorising previous trajectories and then using that information to plan future trajectories. Numerous cortical regions are implicated in successful performance of this task, most notably the hippocampus and mPFC [44,61].

Using this behavioural paradigm, we have shown that alternation deficits and hippocampal/mPFC neural dysfunction segregate with different regions of homology in the DS models. First, we found that alternation rate, a putative index of mnemonic function, was decreased in Dp10Yey mice. In contrast, trial latency, which provides an independent measure of cognitive processing that includes decision-making, planning, goal-directed behaviour, and attention [42,43,45], was prolonged in Dp1Tyb mice. In addition, we have shown that Dp1Tyb mice have a lower peak frequency in the theta band in hippocampus and mPFC, an increase in phase-amplitude coupling between theta and high gamma in hippocampus, and a striking increase in theta phase coupling between mPFC and hippocampus – each of which is independent of the observed differences in movement statistics between Dp1Tyb animals and their WT littermates. Conversely, Dp10Yey mice exhibit decreased phase-amplitude coupling between theta and low gamma in the hippocampus; while Dp17Yey mice did not show any significant behavioral deficits in spatial alternation, or any alteration in the electrophysiology of hippocampus or mPFC. Crucially, the alterations in behavior and neural dynamics observed in our mutant mice are also unlikely to arise from differences in womb-environment, rearing or housing conditions, as we found no differences between WT littermate groups either behaviorally or physiologically.

Previous studies that have interrogated hippocampal function in similar mutant mouse populations [62–65] have found no impairments in long-term spatial memory in Dp10Yey mice [62,63]. In contrast, we observed decreased alternation rates in Dp10Yey mice suggestive of a spatial memory deficit [39]. These conflicting findings likely reflect subtle differences in the behavioral tasks employed, which emphasize complementary aspects of neural processing both within the hippocampus and among a wider network of functionally integrated brain regions, and should be the subject of further investigation [66–68]. The behavioral phenotype observed here was associated with a decrease in theta-gamma phase-amplitude coupling in the hippocampus. It has been well established that spatial memory relies on the periodic reactivation of encoded information by theta modulation of gamma oscillations in rodents [55,69,70] and humans [71–75], and so our finding of decreased gamma-theta coupling in Dp10Yey mice is consistent with their behavioral phenotype, and indicates specific abnormalities of hippocampal circuitry in this model. Our data may thus provide a functional basis for the memory problems evident in people with Down syndrome [7,9,10]. Dp10Yey mice were generated to carry an internal duplication spanning the 39 Hsa21 protein-coding orthologs mapping to Mmu10 and several of these genes, such as *ADAR2*, *S100B*, *CSTB*, *PRMT2*, and

14

378   *TRPM2*, have been shown to play a role in brain development and function, such that aberrant
379   gene dosage may be related to intellectual disability in DS [76,77].

380   An unexpected finding of this study was the delayed decision-making observed in Dp1Tyb
381   mice with preserved memory function. Similar behavioral differences have also been found
382   in humans with DS, who exhibit markedly slower reaction times [78–80]. This impairment has
383   been attributed to deficits in executive function that involve information processing,
384   attention, and inhibition [7,9], resulting in difficulty prioritizing, staying engaged with a task, and
385   consistently responding in the same manner to certain situations [9,81]. Importantly, we found
386   that the increased trial latency observed in these animals was associated with a reduction in
387   theta frequency across both hippocampus and mPFC. It is well established that theta
388   frequency is correlated with running speed in rodents [82], and so a potential explanation for
389   both of these findings is that Dp1Tyb mice simply moved more slowly in general. However,
390   although we found that Dp1Tyb mice spent more time immobile – presumably, reflecting
391   their inability to retain focus on the task - they exhibited no differences in running speed
392   compared to their WT littermates, and the observed reduction in theta frequency was still
393   present when we restricted our analyses to movement periods only.

394   In addition, we found that the delayed decision-making in Dp1Tyb mice was associated with
395   increased hippocampal-mPFC theta coherence. Communication between mPFC and
396   hippocampus occurs through both direct projections and bidirectional pathways via
397   intermediaries in the thalamus, perirhinal and lateral entorhinal cortices [83–85]. It is well
398   accepted that coherence of neuronal activity across brain regions serves as a general
399   mechanism for increasing effective communication during memory and attention tasks.
400   Hippocampal-prefrontal theta-band synchrony facilitates hippocampal inputs to the mPFC
401   and the integration of gamma-mediated cell assemblies in mPFC [26,86]. In addition, theta-band
402   synchrony has frequently been observed during spatial decision-making [35,36]. Thus, our finding
403   of increased hippocampal-mPFC theta coherence is consistent with the observed behavioral
404   phenotype. Widespread increases in low frequency coherence between distributed brain
405   networks, particularly including mPFC, are also observed in people with DS, are more evident
406   in DS than in patients with other neurological disorders, and are inversely related to cognitive
407   performance [15].

408   *DYRK1A*, located on chromosome 21, is a major candidate protein-coding gene for several
409   aspects of DS and encodes a kinase involved in neurodevelopment [46–51]. Overexpression of
410   this gene in transgenic mice results in changes in inhibitory circuits in the mPFC [16,52] and may
411   result in abnormal neural dynamics, particularly in the gamma band. Furthermore, *Dyrk1a*
412   overexpression in mice induces learning and memory impairments detectable in the Morris
413   water maze and Y-maze [52]. Here, we showed that reducing *Dyrk1a* to the normal two copies
414   in Dp1Tyb mice failed to rescue the prolonged decision-making we observed in the spatial
415   alternation task. Thus *Dyrk1a* overexpression is not required for this phenotype, leading us to
416   conclude that another gene or genes, when present in three copies within the Dp1Tyb region,
417   are involved in the abnormal decision-making behavior described here. This is an important
418   result that may, in part, explain why most of the current competitive DYRK1A inhibitors fail
419   to pass the pre-clinical stage with respect to improvement of cognitive impairments in DS [87].
420   Of the 148 protein coding genes within the region duplicated in Dp1Tyb mice, a handful are
421   candidates for further exploration.

422   We note that there may also be critical effects from dosage sensitivity of non-protein coding
423   elements on Hsa21 and our genetically unbiased approach will allow us to map to the DNA

424 region, not to simply focus on the relatively limited set of protein coding elements for which
425 we have functional information. Finding the genes (coding and non-coding) responsible for
426 the cognitive and electrophysiological phenotypes observed in these mice has the
427 translational potential to reveal important routes towards phenotype modifying therapies,
428 for example, by antisense oligomers, but our results indicate that targeting a single gene is
429 unlikely to be sufficient.

430 In summary, our study elucidates an important link between different regions of Hsa21,
431 cognitive deficits and both local and long-range neural circuit dysfunction. Importantly, our
432 results imply that specific cognitive deficits in Down syndrome may result from different
433 underlying genetic, functional and regional abnormalities. This has important implications for
434 understanding such cognitive deficits and indicates that therapies in Down syndrome will
435 likely need to target multiple processes.

436

Acknowledgements

447

Author contributions

449 P.C. collected behavioural and electrophysiology data; P.C, D.B., N.S., analysed
450 electrophysiology data; P.C., N.S., S.N. analysed histology data; F.K.W., V.L.J.T., E.M.C.F.
451 provided mice for this study; S.S., M.G., T.C., N.B., M.C.W., E.M.C.F. helped direct the study;
452 all authors contributed to the manuscript which was primarily drafted by P.C., D.B, M.C.W.,
453 E.M.C.F.

454

Declaration of Interests

456 The authors declare no competing interests.

STAR Methods

Mouse Cohorts including Breeding and Ethics

We examined four mouse strains with the following alleles, previously described in [37,38,49]: C57BL/6J.129P2-Dp(16Lipi-Zbtb21)1TybEmcf/Nimr (hereafter referred to as Dp1Tyb); B6;129S7-Dp(10Prmt2-Pdxk)2Yey/J (hereafter referred to as Dp10Yey); B6.129S7 Dp(17Abcg1-Rrp1b)1Yey (hereafter referred to as Dp17Yey) and B6.129P2-*Dyrk1a*[tm1Mla]. Dp1Tyb, Dp10Yey, Dp17Yey animals were maintained within a facility at University College London, whereas mice for the Dp1Tyb x *Dyrk1a*[tm1Mla/+] intercross were bred at the Francis Crick Institute, to generate Dp1Tyb*Dyrk1aKO mice in which both alleles were on the same chromosome following a genetic crossover. All strains were maintained in separate colonies as hemizygous mutants backcrossed for over ten generations to C57BL/6J, with age- matched WT littermates used as controls. All experiments were undertaken blind to genotype, which was decoded after experimental analysis and reconfirmed using an independent DNA sample isolated from post-mortem tail.

All experiments were performed in accordance with the United Kingdom Animal (Scientific Procedures) Act 1986. Reporting is based on the ARRIVE Guidelines for Reporting Animal Research developed by the National Centre for Replacement, Refinement and Reduction of Animals in Research, London, United Kingdom. Mice were housed in controlled conditions in accordance with guidance issued by the Medical Research Council in Responsibility in the Use of Animals for Medical Research (1993) and all experiments were carried out under License from the UK Home Office and with Local Ethical Review panel approval. Mice were housed in individually ventilated cages (IVC) of 2-5 age-matched animals under controlled environmental conditions (24–25°C; 50–60% humidity; 12 h light/dark cycle) with free access to food and water.

Surgical Preparation and Transmitter Implantation for Long-term Recording

Mice were anaesthetised with 2.5-3 % isoflurane (Abbot, AbbVie Ltd., Maidenhead, UK) in 100% oxygen (flow rate of 1-1.5 litre/min) via gas anaesthesia mask (Model 906, David Kopf Instruments Tujunga, CA, USA) from a recently calibrated vaporizer (Harvard Apparatus, Cambridge, MA). Body temperature was maintained with a heat blanket during surgery. A transmitter (A3028A, Open Source Instruments, Brandeis, Boston, USA)[88] was implanted subcutaneously with the depth recording electrodes (J-electrode, a teflon-insulated stainless steel electrode, Open Source Instruments, Brandeis, Boston, USA) positioned in mPFC (1.8 mm anterior, 0.4 mm lateral, 1.5 mm ventral) and dorsal hippocampus (1.85 mm posterior, 1.25 mm lateral, 1.45 mm ventral) [89,90]. The reference electrode was implanted over the cerebellum posterior to lambda. The whole assembly was held in place with dental cement (Simplex Rapid, Acrylic Denture Polymer, UK). A subcutaneous injection of bupivacaine and metacam was provided for post-surgical pain management. At the end of surgery, enrofloxacin (5mg/kg, Baytril, Bayer health care) and pre-warm saline (0.5-1 ml) were administered subcutaneously. The animals were placed in a temperature controlled (25°C) recovery chamber until ambulatory and closely monitored at least 1-2 hours before returning to their home cage to allow recovery for at least 14 days after surgery.

The transmitter, which has no adverse effects[91], was chronically implanted for longitudinal data recordings. During all recording sessions, continuous LFP recordings were recorded

17

502 (bandpass filter: 0.2 Hz to 160 Hz, 512Hz sampling rate with 16 bit resolution) using LWDAQ
503 Software (Open Source Instruments, Brandeis, Boston, USA). Animals were carefully
504 monitored daily and were euthanized at the end of experiment with pentobarbital (25
505 mg/kg).

506

507 **Behavioural Testing: T-maze Spontaneous Alternation**

508 Cognitive function in male mice from each strain and associated age-matched WT controls
509 was assessed using the spontaneous alternation paradigm in an enclosed T-maze apparatus
510 [39]. Animals were transferred to the testing room for 1-2 hours before each experiment to
511 habituate to the environment and achieve an optimal state of arousal. Each mouse was then
512 subjected to ~10 trials per session, and sessions were completed at 3, 6, and 9 months of age
513 (see Supplementary Tables 1 and 3 for average trial numbers in each group).

514 During each trial, the animal was first placed in the start chamber for 100s while reference
515 phase LFP was recorded. Next, the guillotine door separating the start chamber from the
516 central arm was raised and the mouse was allowed to run and choose a goal arm. After making
517 a choice, the guillotine doors separating the central arm from each goal arm were slowly
518 lowered, such that the animal was confined in the chosen goal arm which it could then explore
519 for 30s. Next, the animal was transferred back to the start chamber, the guillotine door
520 separating the central arm from the goal arms was raised and, after another 100s delay period
521 in the start chamber, the guillotine door separating the start chamber from the central arm
522 was raised again to allow the mouse a choice between the two open goal arms. Importantly,
523 each trial included a free choice of goal arms on both the sample run and choice run (Figure
524 1a and Supplementary Figure 1a, b).

525 Trials were marked as successful if the mouse chose different goal arms on each run, and
526 failures if the mouse chose the same goal arm on both runs. Alternation rate was defined as
527 the total proportion of successful trials for each animal during each session. Trial latency was
528 calculated as the time between the door isolating the start chamber being raised and the time
529 at which the animals nose reached the decision point (i.e. exiting the central arm of the T-
530 maze) immediately prior to the whole body completely entering the goal arm (indicative of a
531 choice being made; see Figure 1b). This ensures that 'vicarious trial and error' behaviour, in
532 which animals approach the decision point and look along either choice arm prior to making
533 a decision, is excluded. Trial data was discarded if the latency on either run exceeded 120s.

534 Movement statistics were extracted from video data that covered the central arm, decision
535 point, and initial stages of each goal arm, sampled at a rate of 25Hz, using the single mouse
536 tracker plugin for Icy [92]. Running speed values were smoothed with a box car filter of 400ms
537 width, and periods of immobility were defined as time frames when the animal's movement
538 speed was lower than 2cm/s.

539

540 **Histology**

541 At the end of the experiment, the brain was removed and immediately immersed in 4%
542 paraformaldehyde for >24 hours before being transferred to 30% sucrose post-fixation
543 solution. Brain sections (40-μm thick thickness) were cut using a microtome (Leica SM2000R,
544 Leica Microsystems ltd., United Kingdom) and stained with cresyl violet to allow histological

545 location of the electrode track. This procedure allowed us to verify recording electrode
546 locations, and LFP data were only included in the study if electrode tips were located in mPFC
547 and dorsal hippocampus. In total, LFP data from just one animal was excluded because the
548 recording site was outside the target region (Supplementary Figure 5).

549

550 **EEG Data Analysis**

551 *LFP Pre-processing*

552 For our initial analyses, continuous LFP recordings from each region were segmented into 10s
553 epochs that lasted from 5s before to 5s after animals reached the decision point on each run
554 (plus 1s padding, subsequently discarded to account for potential edge effects). Each epoch
555 was visually inspected for artefacts prior to further analysis using custom written Matlab
556 (Mathworks, Natick MA) code (see Supplementary Tables 1 and 3 for trial numbers across
557 strains). Trial latency and alternation rate data from trials excluded due to LFP artefacts were
558 nonetheless included in behavioural analyses.

559 For subsequent analyses in which the relationship between movement statistics and EEG
560 features were examined, continuous LFP recordings from each region were segmented to
561 match the available movement data (plus 1s padding, subsequently discarded to account for
562 potential edge effects). Any epochs that exhibited artefacts during visual inspection or for
563 which video data (and therefore movement statistics) was either incomplete or unavailable
564 were excluded from subsequent analysis.

565

566 *Time-frequency Analysis*

567 After de-trending and de-meaning the LFP signal from each trial, time-frequency
568 decomposition was performed using a five cycle complex Morlet wavelet transform, with 1s
569 of data from the beginning and end of each epoch subsequently discarded to avoid edge
570 effects. Time-frequency representations were then averaged across this time window to
571 provide a power spectrum for each epoch, and each power spectrum was then normalised by
572 its integral to facilitate comparisons between animals. Finally, these normalised power values
573 were averaged across the 6-12Hz theta band to provide an index of theta power in each epoch
574 for statistical comparison.

575 In addition, to characterise the relationship between theta power and movement, we zero-
576 phase filtered each LFP signal in the 6-12Hz theta band using a 400th order finite impulse
577 response (FIR) filter, discarded 1s of data from the beginning and end of the signal to avoid
578 edge effects, extracted the analytic signal using the Hilbert transform, and then computed
579 dynamic power and frequency. Running speed data was up-sampled to match the power and
580 frequency time series, allowing us to compute average theta power during movement periods
581 only and to estimate the intercept and slope of the running speed v theta frequency
582 relationship in each animal using linear regression.

583

584 *Phase-amplitude Coupling Analysis*

585 To assay phase–amplitude coupling in the hippocampal LFP signal, we first computed cross-
586 frequency coherence across a range of phase and amplitude frequencies following [54]. To do

587 so, we extracted the amplitude at each time point across a frequency range of 20-160Hz from
588 the Morlet wavelet transform described above, and then computed coherence between the
589 original LFP signal and each of these amplitude time series across a phase frequency range of
590 2-40Hz using a window size of 1s and an overlap between subsequent windows of 0.5s. These
591 coherence spectra subsequently index phase-amplitude coupling (PAC) between low
592 frequency phase and high frequency amplitude, and can be aggregated across amplitude
593 frequencies to generate the cross-frequency coherence images shown in Figure 3 and
594 Supplementary Figure 7.

595 Visual inspection of cross-frequency coherence images averaged across all animal groups
596 (shown in Supplementary Figure 7) revealed that 6-12Hz theta phase modulated the
597 amplitude of higher frequency oscillations in two distinct bands, 60-120Hz (hereafter referred
598 to as 'low gamma', LG) and 140-160Hz (hereafter referred to as 'high gamma', HG). We
599 subsequently characterised the magnitude of theta-LG and theta-HG PAC in each epoch by
600 zero-phase filtering the LFP signal separately in the 6-12Hz theta, 60-120Hz LG and 140-160Hz
601 HG bands using a 400th order FIR filter, extracting the analytic signal in each band using the
602 Hilbert transform, and then computing the mean amplitude of the higher frequency
603 oscillations in each of 30 evenly distributed theta phase bins. The resulting vector length of
604 each mean amplitude distribution, computed using the circular statistics toolbox for Matlab
605 [93], provides an index of theta-LG and theta-HG PAC in each epoch for statistical comparison.

606

Phase Coupling Analysis

608 To compute an index of theta phase coherence between LFP recordings from the
609 hippocampus and mPFC in each epoch, we first generated coherence spectra for each epoch
610 using a window size of 1s and an overlap between subsequent windows of 0.5s and then
611 averaged coherence values across the 6-12Hz theta range. In addition, to estimate the theta
612 phase lag between concurrent oscillations in these regions, we zero-phase filtered each LFP
613 signal in the 6-12Hz theta band using a 400th order FIR filter, discarded 1s of data from the
614 beginning and end of the signal to avoid edge effects, extracted the analytic signal using the
615 Hilbert transform, and then computed the circular mean theta phase difference between
616 regions across all time points within each epoch. This provides an indication of the time lag
617 between those signals in the 6-12Hz theta band (computed by dividing the phase difference
618 by the angular frequency at the centre of the theta band, i.e. 18π rad/s).

619

Correcting for Differences in Movement Statistics

621 Where significant differences in movement statistics between groups existed, we
622 attempted to eliminate any potential confound on concomitant differences in theta
623 coherence and theta-gamma PAC by linear regression. Specifically, we extracted the
624 residual coherence or PAC values after regressing the amount of time spent immobile
625 against those parameters across all animals (mutant and WT), and then assessed the
626 difference in residual values between groups.

Statistical Analysis

Detailed statistical analysis was performed using SPSS 24 (Statistical Product and Service Solutions, IBM). All data are presented as mean ± SEM. Comparisons of means were performed using two-tailed Student's t test and one way ANOVA with Tukey post hoc test if the data were normally distributed; Wilcoxon Signed test, Friedman's test, or Mann-Whitney U-test if the data were not normally distributed (with the Shapiro-Wilk test and Kolmogorov-Smirnov test with Lillefors correction used to assess normality of the data distributions). Generalized linear model (GLM) Type III tests followed by Bonferroni post hoc tests were used for analysis of repeated measures longitudinal data. For circular (i.e. phase lag) data, the Watson-Williams test was used to assess differences between groups [93]. Differences were considered statistically significant at $p < 0.05$. For full details of all statistical analyses, please refer to Supplementary Table 2.

639   **Supplementary Information**

640
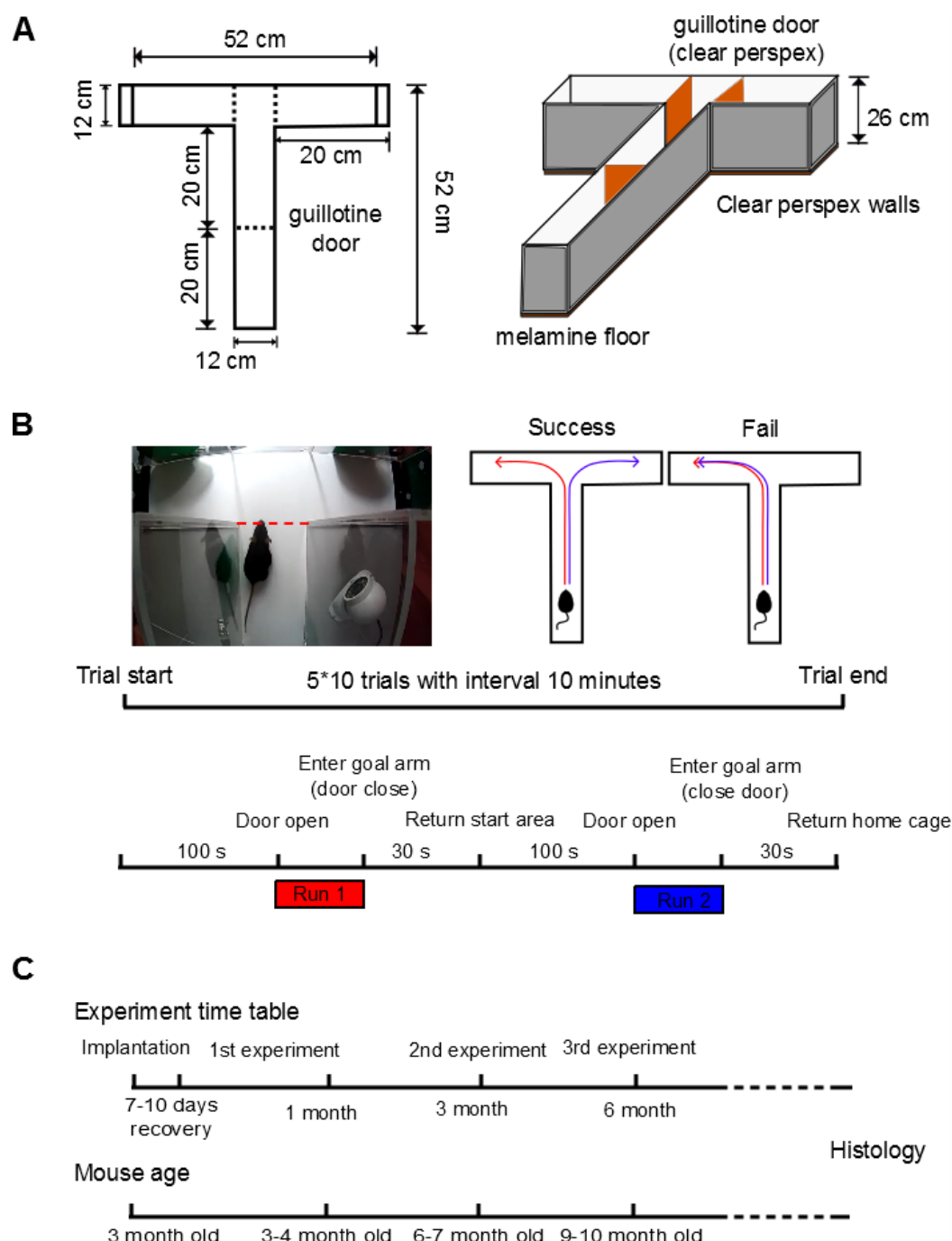
641   **Supplementary Figure 1: Further Details of the Behavioural Protocol**

642   Experimental protocol for the T-maze spontaneous alternation task, showing: **(a)** a schematic of the
643   T-maze; **(b)** the trial protocol for probing spontaneous alternation behaviour maze; and **(c)** a time line
644   for the longitudinal study.

645
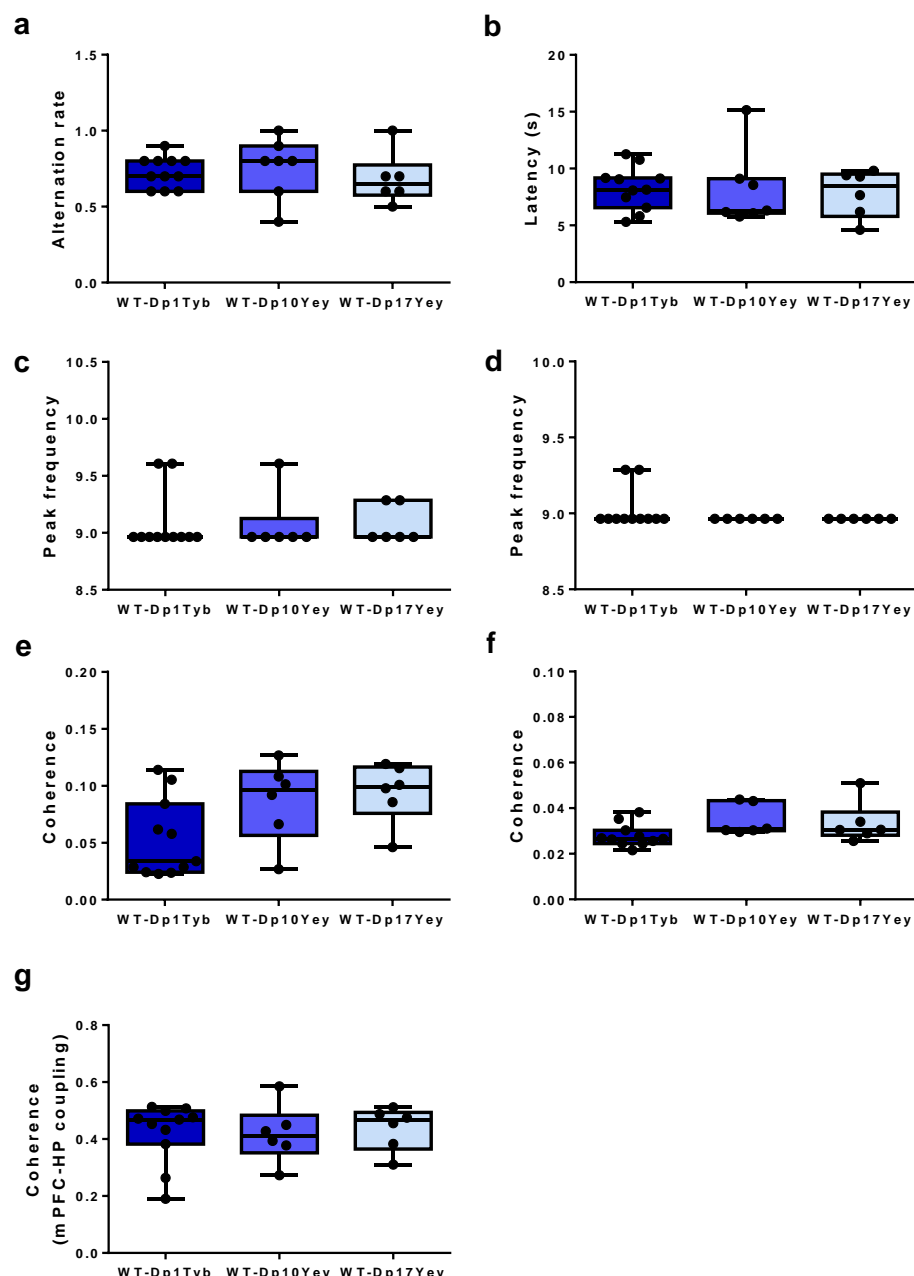
Supplementary Figure 2: Comparison of behavioural and physiological data across WT groups

Comparison of **(a)** spatial alternation rate; **(b)** trial latency; peak theta frequency in **(c)** hippocampus and **(d)** medial prefrontal cortex (mPFC); **(e)** theta-low gamma and **(f)** theta-high gamma phase-amplitude coupling in the hippocampus; and **(g)** theta coherence between hippocampus and mPFC across WT cohorts. Data are presented as box-whisker plots indicating the median, 25th and 75th percentiles, minimum and maximum values, with data for individual mice superimposed. There are no significant differences between WT groups in any panel. Please refer to Supplementary Table 2 for full details of all statistical analyses.

23
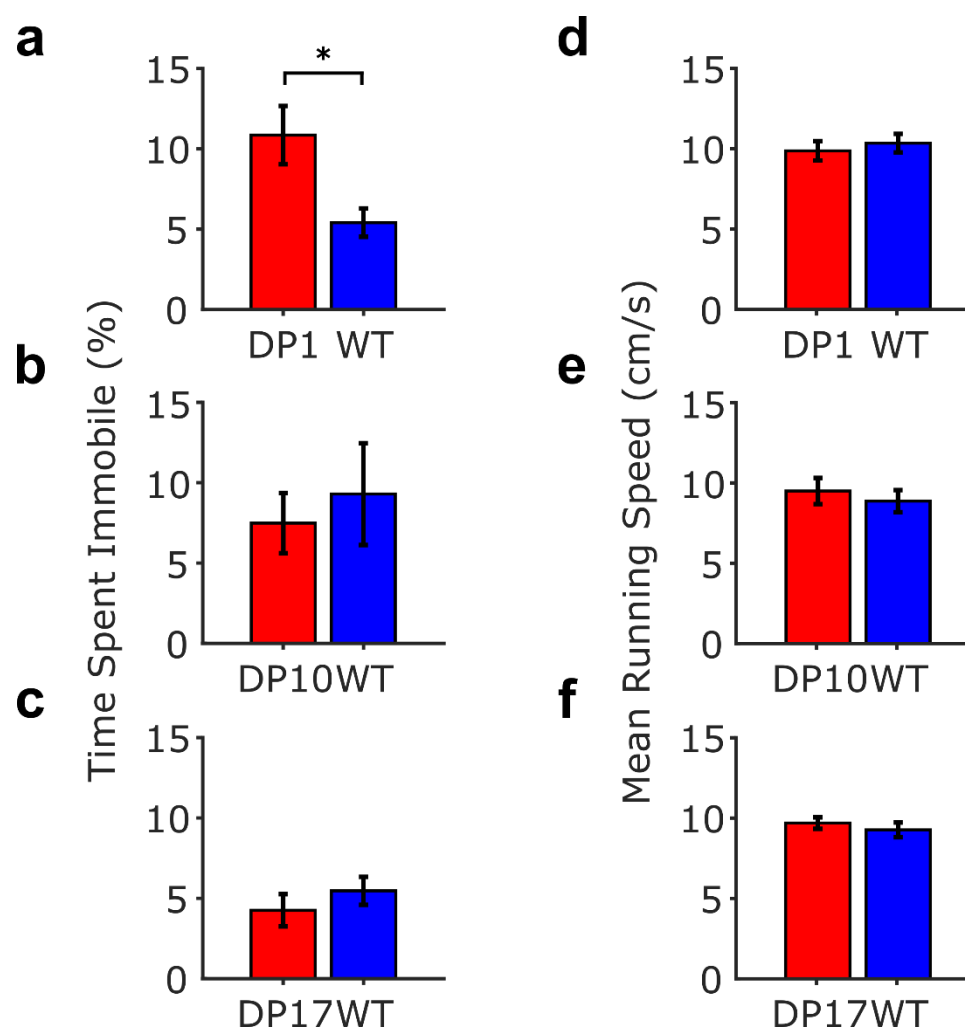
Supplementary Figure 3: Comparison of movement statistics across groups

(a-c) Relative period of each trial spent immobile (i.e. running speed <2cm/s); and **(d-f)** the average running speed during movement (i.e. running speed ≥2cm/s) across all mutant mouse and WT control groups. These data illustrate that the increased trial latency observed in Dp1Tyb mice results from significantly more time spent immobile ($t(13)=2.46$, $p<0.05$) without any difference in mean running speed during movement ($t(13)=-0.49$, $p=0.63$). No differences in time spent immobile or mean running speed during movement were observed in any other group compared to their WT cohort (all $p>0.38$), or between any of the WT groups (both $p>0.24$). Please refer to Supplementary Table 2 for full details of all statistical analyses.
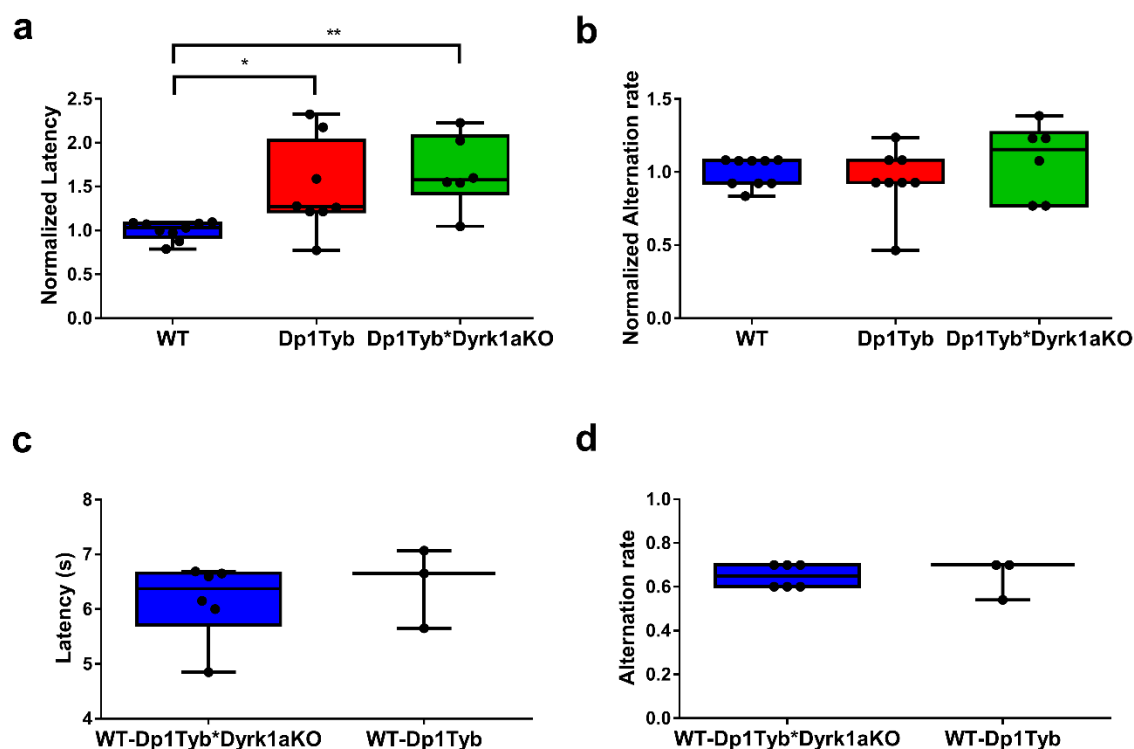
Supplementary Figure 4: Behavioural performance in Dp1Tyb and Dp1Tyb*Dyrk1aKO mice

(a) Alternation rate and **(b)** trial latency averaged over 10 trials for Dp1Tyb and Dp1Tyb*Dyrk1aKO mice compared to their pooled wild-type (WT) control group. All data are normalized to the WT mean. Trial latency differs significantly between groups (One way ANOVA, F(2,20)=6.21, p<0.0001). Post-hoc Tukey HSD indicates that trial latency is significant longer in Dp1Tyb and Dp1Tyb*Dyrk1aKO mice, compared to pooled WT (p<0.05 and p<0.01, respectively). **(c)** Comparison of trial latency and **(d)** alternation rate between WT cohorts, illustrating no significant differences in either case (Kruskal-Wallis test, both p>0.58). Data are presented as box-whisker plots indicating the median, 25th and 75th percentiles, minimum and maximum values, with data for individual mice superimposed. Please refer to Supplementary Table 2 for full details of all statistical analyses.
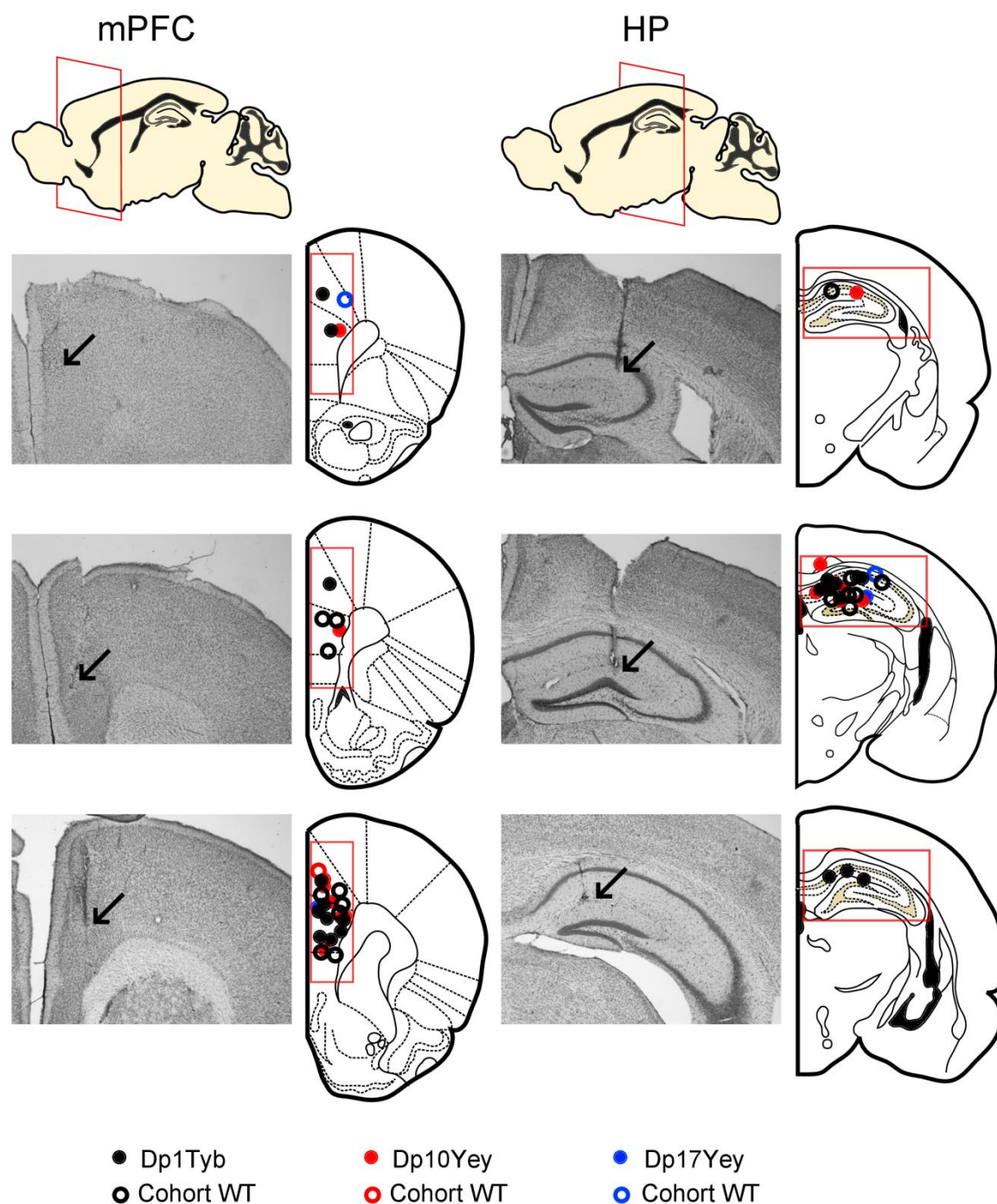
Supplementary Figure 5: Histology

Coronal sections of Nissl stained brains showing typical locations of recording electrode tips in medial prefrontal cortex and dorsal hippocampus. Arrows indicate the tip of each recording electrode. LFP data were only included in the study if electrode tips were located in mPFC (indicated by coloured rectangle) and dorsal hippocampus (HP, also indicated by coloured rectangle).
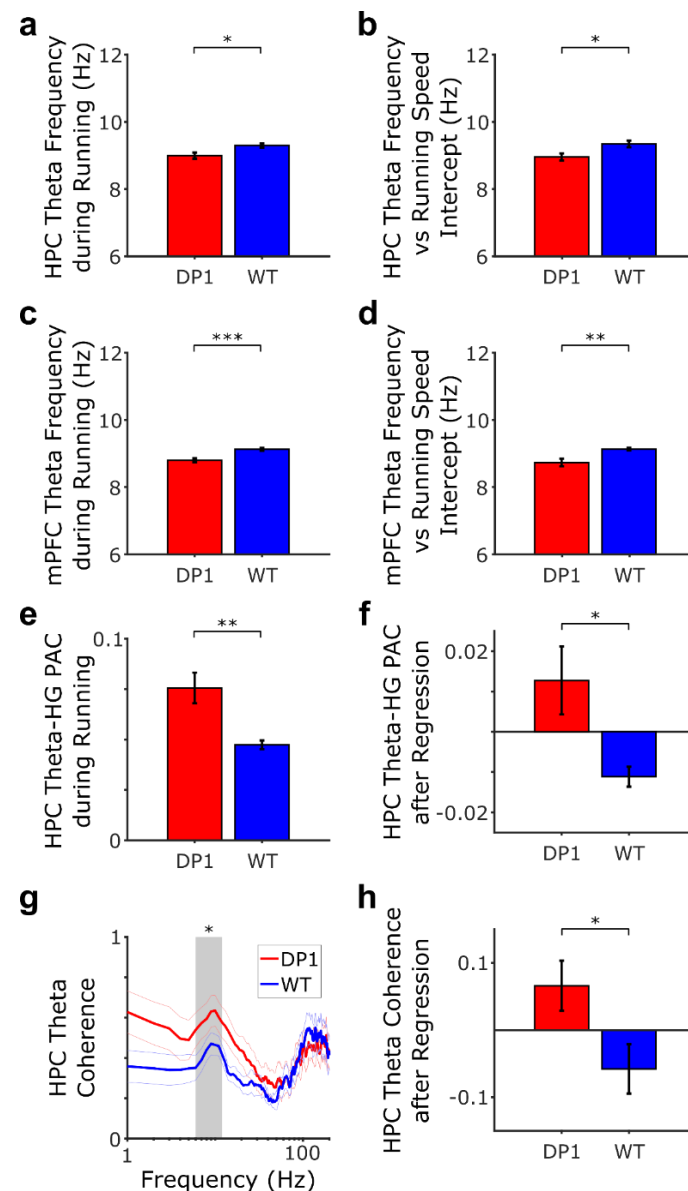
Supplementary Figure 6: Details of Dp1Tyb analyses controlling for movement statistics

(a,c) Average theta frequency and **(b,d)** intercept of the running speed v theta frequency relationship during movement for Dp1Tyb and WT groups in **(a,b)** hippocampus (HPC) and **(c,d)** medial prefrontal cortex (mPFC). Theta frequency during movement is significantly lower in Dp1 animals in both HPC (t(13)=-2.80, p<0.05) and mPFC (t(13)=-4.52, p<0.001), due to a reduction in the intercept (HPC: t(13)=-2.68, p<0.05; mPFC: t(13)=-3.45, p<0.01) but not the slope (both p>0.24, data not shown) of the running speed v theta frequency relationship. **(e)** Average theta-HG PAC in HPC is significantly higher in Dp1 animals when analyses are restricted to movement periods only (t(13)=3.12, p<0.01). **(f)** Moreover, the influence of average time immobile on theta-HG PAC is removed by linear regression across animals, the difference between groups is still significant (t(13)=2.88, p<0.05). **(g)** Average theta coherence between HPC and mPFC is significantly higher in Dp1 animals when analyses are restricted to movement periods only (t(13)=2.44, p<0.05). **(h)** Moreover, if the influence of average time immobile on theta coherence is removed by linear regression across animals, the difference between groups is still significant (t(13)=2.36, p<0.05). Please refer to Supplementary Table 2 for full details of all statistical analyses.

699
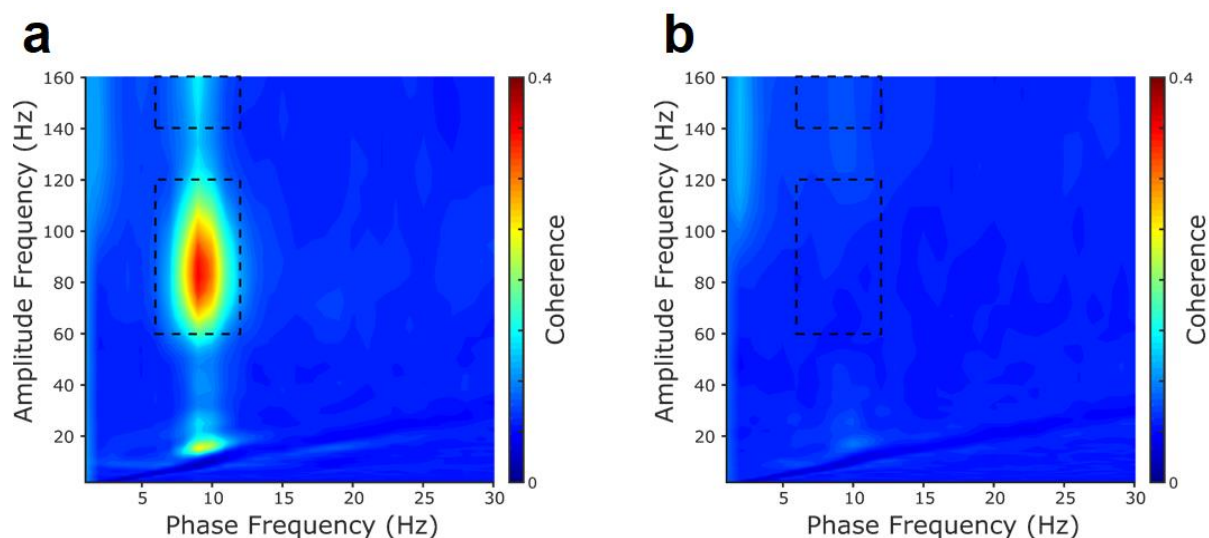
Supplementary Figure 7: Average phase-amplitude comodulograms across all animals

Phase-amplitude comodulograms, averaged across all DS model and WT control groups at 3 months of age for **(a)** hippocampus and **(b)** mPFC. Visual inspection reveals strong peaks between 6-12Hz theta phase and both 60-120Hz 'low gamma' (LG) and 140-160Hz 'high gamma' (HG) rhythms in the hippocampus, with no strong phase-amplitude coupling apparent in the mPFC (see Figure 3 for details of comparisons between groups).
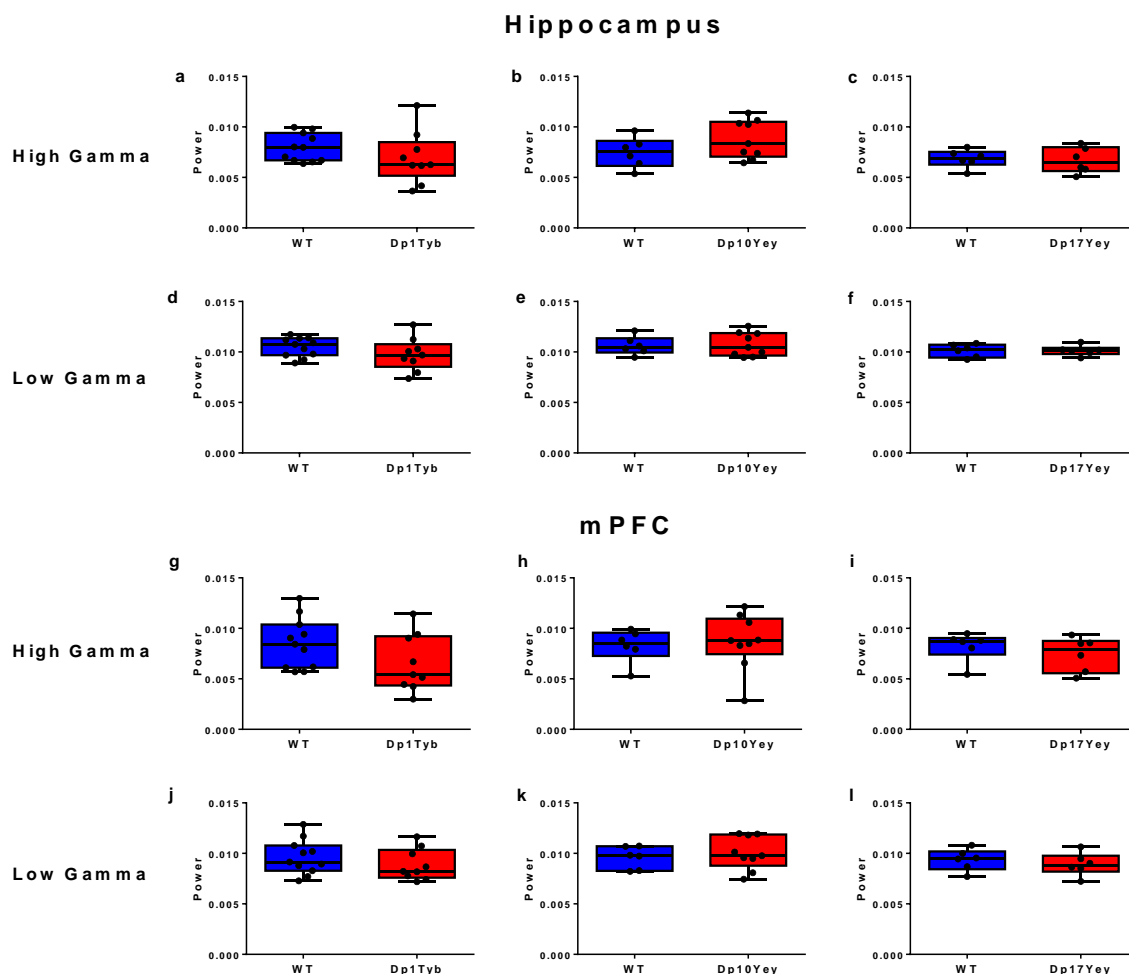
Supplementary Figure 8: Comparison of Gamma Power between Groups

Average power in the low (60-120Hz) and high (120-140Hz) gamma bands in **(a-f)** hippocampus and **(g-l)** mPFC for **(a,d,g,j)** Dp1Tyb and WT; **(b,e,h,k)** Dp10Yey and WT; **(c,f,i,l)** Dp17Yey and WT animals during spontaneous alternation on the T-maze, which show no significant differences between mutant mice and WT groups in any instance. Data are presented as box-whisker plots indicating the median, 25th and 75th percentiles, minimum and maximum values, with data for individual mice superimposed. Please refer to Supplementary Table 2 for full details of all statistical analyses.
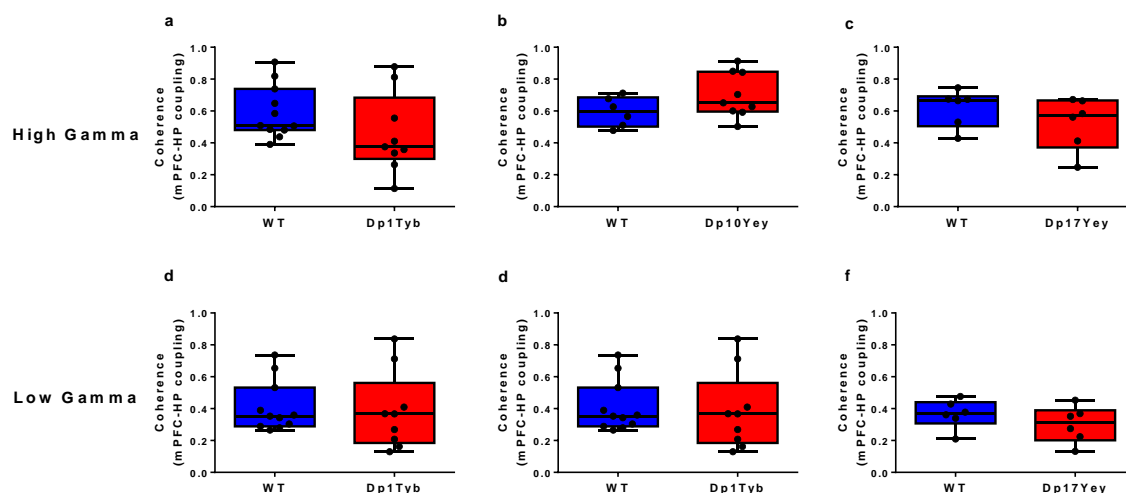
Supplementary Figure 9: Comparison of Gamma Coherence between Groups

Hippocampal-medial prefrontal coherence in the **(a-c)** high- and **(d-f)** low- gamma frequency bands for each mutant mouse and WT control group, which show no significant differences in any instance. Data are presented as box-whisker plots indicating the median, 25th and 75th percentiles, minimum and maximum values, with data for individual mice superimposed. Please refer to Supplementary Table 2 for full details of all statistical analyses.

721   **Supplementary Table 1: Summary of Trial and Animal Numbers at 3 months of Age**

	Summary						
	Dp1Tyb	**WT**	**Dp10Yey**	**WT**	**Dp17Yey**	**WT**	**Mean**
n	9	11	10	6	6	6	8
All Trials (Mean)	9.33	8.64	8.70	7.83	10.17	9.83	9.08
All Trials (SD)	2.00	2.38	2.11	2.79	0.41	0.41	1.68
Artefact Trials (Mean)	2.00	1.73	1.80	0.50	1.00	0.33	1.23
Artefact Trials (SD)	2.74	2.33	2.66	1.22	0.89	0.82	1.78
Trials Included (Mean)	7.33	6.91	6.90	7.33	9.17	9.50	7.86
Trials Included (SD)	2.69	2.30	3.63	2.58	0.98	0.84	2.17

722

723 **Supplementary Table 2: Full Details of all Statistical Analyses**

		Figure 1			
	N	Test	Test value	p value	Post-hoc test
Figure 1d	WT=11 Dp1Tyb=9	Unpaired t-test (two tailed)	t(18)=1.50	0.15	NA
Alternation v chance	WT=11	Wilcoxon signed test	Z=-2.96	**<0.001**	NA
Alternation v chance	Dp1Tyb=9	Wilcoxon signed test	Z=-2.39	**<0.01**	NA
Figure 1e	WT=7 Dp10Yey=9	Unpaired t-test (two tailed)	t(14)=2.50	**<0.05**	NA
Alternation v chance	WT=7	Wilcoxon signed test	Z=-2.22	**<0.05**	NA
Alternation v chance	Dp10Yey=9	Wilcoxon signed test	Z=-1.39	0.11	NA
Figure 1f	WT=6 Dp17Yey=6	Unpaired t-test (two tailed)	t(10)=1.05	0.32	NA
Alternation v chance	WT=6	Wilcoxon signed test	Z=-2.04	**<0.05**	NA
Alternation v chance	Dp17Yey=6	Wilcoxon signed test	Z=-2.04	**<0.05**	NA
Figure 1g	WT=11 Dp1Tyb=9	Unpaired t-test (two tailed)	t(18)=5.97	**<0.001**	NA
Figure 1h	WT=7 Dp10Yey=9	Unpaired t-test (two tailed)	t(14)=1.59	0.14	NA
Figure 1i	WT=6 Dp17Yey=6	Unpaired t-test (two tailed)	t(10)=1.25	0.24	NA

724

Figure 2					
	N	Test	Test value	p value	Post-hoc test
Figure 2a Theta power	WT=11 Dp1Tyb=9	Unpaired t-test (two tailed)	t(18)=1.18	0.25	NA
Figure 2a Theta freq.	WT=11 Dp1Tyb=9	Mann-Whitney (two tailed)	U=22.5	**0.012**	NA
Figure 2b Theta power	WT=6 Dp10Yey=9	Unpaired t-test (two tailed)	t(13)=0.59	0.57	NA
Figure 2b Theta freq.	WT=6 Dp10Yey=9	Mann-Whitney (two tailed)	U=23.0	0.65	NA
Figure 2c Theta power	WT=6 Dp17Yey=6	Unpaired t-test (two tailed)	t(10)=0.59	0.57	NA
Figure 2c Theta freq.	WT=6 Dp17Yey=6	Mann-Whitney (two tailed)	U=12.0	0.45	NA
Figure 2d Theta power	WT=11 Dp1Tyb=9	Unpaired t-test (two tailed)	t(18)=1.74	0.10	NA
Figure 2d Theta freq.	WT=11 Dp1Tyb=9	Mann-Whitney (two tailed)	U=13.5	**0.001**	NA
Figure 2e Theta power	WT=6 Dp10Yey=9	Unpaired t-test (two tailed)	t(13)=0.59	0.57	NA
Figure 2e Theta freq.	WT=6 Dp10Yey=9	Mann-Whitney (two tailed)	U=27.0	> 0.9999	NA
Figure 2f Theta power	WT=6 Dp17Yey=6	Unpaired t-test (two tailed)	t(10)=0.45	0.66	NA
Figure 2f Theta freq.	WT=6 Dp17Yey=6	Mann-Whitney (two tailed)	U=18.0	> 0.9999	NA

725

33

Figure 3					
	N	**Test**	**Test value**	**p value**	**Post-hoc test**
Figure 3a Theta-LG	WT=11 Dp1Tyb=9	Mann-Whitney (two tailed)	U=44.0	0.70	NA
Figure 3a Theta-HG	WT=11 Dp1Tyb=9	Mann-Whitney (two tailed)	U=16.0	**<0.01**	NA
Figure 3b Theta-LG	WT=6 Dp10Yey=9	Mann-Whitney (two tailed)	U=8.0	**0.026**	NA
Figure 3b Theta-HG	WT=6 Dp10Yey=9	Mann-Whitney (two tailed)	U=16.0	0.22	NA
Figure 3c Theta-LG	WT=6 Dp17Yey=6	Mann-Whitney (two tailed)	U=15.0	0.68	NA
Figure 3c Theta-HG	WT=6 Dp17Yey=6	Mann-Whitney (two tailed)	U=16.0	0.79	NA

726

Figure 4					
	N	**Test**	**Test value**	**p value**	**Post-hoc test**
Figure 4a	WT=11 Dp1Tyb=9	Mann-Whitney (two tailed)	U=11.0	**0.002**	NA
Figure 4b	WT=6 Dp10Yey=9	Mann-Whitney (two tailed)	U=24.0	0.77	NA
Figure 4c	WT=6 Dp17Yey=6	Mann-Whitney (two tailed)	U=17.0	0.90	NA

727

34

Figure 5					
	N	Test	Test value	p value	Post-hoc test
Figure 5a	WT=6 Dp1Tyb=4	GLM Type III tests	Genotype $\chi^2(1)=56.097$	**<0.001**	NA
			Age $\chi^2(2)=30.474$	**<0.001**	NA
			Genotype*age $\chi^2(2)=17.270$	**<0.001**	NA
Figure 5b	WT=6 Dp1Tyb=4	GLM Type III tests	Genotype $\chi^2(1)=6.843$	**0.009**	NA
			Age $\chi^2(2)=2.780$	0.25	NA
			Genotype*age $\chi^2(2)=0.094$	0.95	NA
Figure 5c	WT=6 Dp1Tyb=4	GLM Type III tests	Genotype $\chi^2(1)=8.934$	**0.008**	NA
			Age $\chi^2(2)=0.377$	0.83	NA
			Genotype*age $\chi^2(2)=2.806$	0.25	NA
Figure 5d	WT=6 Dp1Tyb=4	GLM Type III tests	Genotype $\chi^2(1)=14.284$	**<0.001**	NA
			Age $\chi^2(2)=7.958$	**0.019**	NA
			Genotype*age $\chi^2(2)=0.932$	0.33	NA
Figure 5e	WT=6 Dp1Tyb=4	GLM Type III tests	Genotype $\chi^2(1)=29.63$	**<0.001**	NA
			Age $\chi^2(2)=9.27$	**0.01**	NA
			Genotype*age $\chi^2(2)=0.389$	0.82	NA
Figure 5f	WT=4 Dp10Yey=5	GLM Type III tests	Genotype $\chi^2(1)=12.530$	**<0.001**	NA
			Age $\chi^2(2)=16.541$	**<0.001**	NA
			Genotype*age $\chi^2(2)=2.087$	0.35	NA
Figure 5g	WT=3 Dp10Yey=4	GLM Type III tests	Genotype $\chi^2(1)=18.239$	**<0.001**	NA
			Age $\chi^2(2)=2.022$	0.36	NA
			Genotype*age $\chi^2(2)=1.156$	0.56	NA

728

35

Supplementary Figure 2					
	N	Test	Test value	p value	Post-hoc test
Supp. Fig. 2a	WT-Dp1Tyb=11 WT-Dp10Yey=6 WT-Dp17Yey=6	One way ANOVA	$F(2,21)=0.38$	0.69	NA
Supp. Fig. 2b	WT-Dp1Tyb=11 WT-Dp10Yey=6 WT-Dp17Yey=6	One way ANOVA	$F(2,21)=0.06$	0.94	NA
Supp. Fig. 2c	WT-Dp1Tyb=11 WT-Dp10Yey=6 WT-Dp17Yey=6	Kruskal-Wallis test	$\chi^2(2)=0.85$	0.65	NA
Supp. Fig. 2d	WT-Dp1Tyb=11 WT-Dp10Yey=6 WT-Dp17Yey=6	Kruskal-Wallis test	$\chi^2(2)=2.29$	0.32	NA
Supp. Fig. 2e	WT-Dp1Tyb=11 WT-Dp10Yey=6 WT-Dp17Yey=6	Kruskal-Wallis test	$\chi^2(2)=5.85$	0.054	NA
Supp. Fig. 2f	WT-Dp1Tyb=11 WT-Dp10Yey=6 WT-Dp17Yey=6	Kruskal-Wallis test	$\chi^2(2)=4.14$	0.13	NA
Supp. Fig. 2g	WT-Dp1Tyb=11 WT-Dp10Yey=6 WT-Dp17Yey=6	Kruskal-Wallis test	$\chi^2(2)=0.86$	0.65	NA

729

Supplementary Figure 3					
	N	Test	Test value	p value	Post-hoc test
Supp. Fig. 3a	WT=8 Dp1Tyb=7	Unpaired t-test (two tailed)	$t(13)=2.46$	**<0.05**	NA
Supp. Fig. 3b	WT=5 Dp10Yey=10	Unpaired t-test (two tailed)	$t(13)=-0.52$	0.61	NA
Supp. Fig. 3c	WT=6 Dp17Yey=6	Unpaired t-test (two tailed)	$t(10)=-0.91$	0.38	NA
Supp. Fig. 3d	WT=8 Dp1Tyb=7	Unpaired t-test (two tailed)	$t(13)=-0.49$	0.63	NA
Supp. Fig. 3e	WT=5 Dp10Yey=10	Unpaired t-test (two tailed)	$t(13)=0.50$	0.63	NA
Supp. Fig. 3f	WT=6 Dp17Yey=6	Unpaired t-test (two tailed)	$t(10)=0.73$	0.48	NA
Time immobile across WT	WT-Dp1Tyb=8 WT-Dp10Yey=5 WT-Dp17Yey=6	One way ANOVA	$F(2,16)=1.58$	0.24	NA
Running speed across WT	WT-Dp1Tyb=8 WT-Dp10Yey=5 WT-Dp17Yey=6	One way ANOVA	$F(2,16)=1.48$	0.26	NA

730

Supplementary Figure 4					
	N	Test	Test value	p value	Post-hoc test
Supp. Fig. 4a	WT=9 Dp1Tyb=8 Dp1Tyb*Dyrk1aKO=6	One way ANOVA	$F_{(2,20)}=6.36$	**<0.01**	Tukey HSD: WT vs. Dp1Tyb **p<0.05**
					WT vs. Dp1Tyb*Dyrk1aKO **p<0.01**
Supp. Fig. 4b	WT=9 Dp1Tyb=8 Dp1Tyb*Dyrk1aKO=6	Kruskal-Wallis test	$\chi^2_{(2)}=0.68$	0.71	NA
Supp. Fig. 4c	WT-Dp1Tyb=3 WT-Dp1Tyb*Dyrk1aKO=6	Unpaired t-test (two tailed)	$t_{(7)}=0.60$	0.57	NA
Supp. Fig. 4d	WT-Dp1Tyb=3 WT-Dp1Tyb*Dyrk1aKO=6	Mann-Whitney (two tailed)	U=9.0	>0.99	NA

731

Supplementary Figure 6					
	N	Test	Test value	p value	Post-hoc test
Supp. Fig. 6a	WT=8 Dp1Tyb=7	Unpaired t-test (two tailed)	$t_{(13)}=-2.80$	**<0.05**	NA
Supp. Fig. 6b	WT=8 Dp1Tyb=7	Unpaired t-test (two tailed)	$t_{(13)}=-2.68$	**<0.05**	NA
Supp. Fig. 6c	WT=8 Dp1Tyb=7	Unpaired t-test (two tailed)	$t_{(13)}=-4.52$	**<0.001**	NA
Supp. Fig. 6d	WT=8 Dp1Tyb=7	Unpaired t-test (two tailed)	$t_{(13)}=-3.45$	**<0.005**	NA
Supp. Fig. 6e	WT=8 Dp1Tyb=7	Unpaired t-test (two tailed)	$t_{(13)}=3.79$	**<0.005**	NA
Supp. Fig. 6f	WT=8 Dp1Tyb=7	Unpaired t-test (two tailed)	$t_{(13)}=2.88$	**<0.05**	NA
Supp. Fig. 6g	WT=8 Dp1Tyb=7	Unpaired t-test (two tailed)	$t_{(13)}=2.44$	**<0.05**	NA
Supp. Fig. 6h	WT=8 Dp1Tyb=7	Unpaired t-test (two tailed)	$t_{(13)}=2.36$	**<0.05**	NA

732

Supplementary Figure 8					
	N	Test	Test value	p value	Post-hoc test
Supp. Fig. 8a	WT=11 Dp1Tyb=9	Unpaired t-test (two tailed)	t(18)=1.11	0.28	NA
Supp. Fig. 8b	WT=6 Dp10Yey=9	Unpaired t-test (two tailed)	t(13)=1.44	0.17	NA
Supp. Fig. 8c	WT=6 Dp17Yey=6	Unpaired t-test (two tailed)	t(10)=0.24	0.81	NA
Supp. Fig. 8d	WT=11 Dp1Tyb=9	Unpaired t-test (two tailed)	t(18)=1.25	0.23	NA
Supp. Fig. 8e	WT=6 Dp10Yey=9	Unpaired t-test (two tailed)	t(13)=0.26	0.80	NA
Supp. Fig. 8f	WT=6 Dp17Yey=6	Unpaired t-test (two tailed)	t(10)=0.001	0.10	NA
Supp. Fig. 8g	WT=11 Dp1Tyb=9	Unpaired t-test (two tailed)	t(18)=1.66	0.11	NA
Supp. Fig. 8h	WT=6 Dp10Yey=9	Unpaired t-test (two tailed)	t(13)=0.30	0.77	NA
Supp. Fig. 8i	WT=6 Dp17Yey=6	Unpaired t-test (two tailed)	t(10)=0.89	0.40	NA
Supp. Fig. 8j	WT=11 Dp1Tyb=9	Unpaired t-test (two tailed)	t(18)=1.01	0.32	NA
Supp. Fig. 8k	WT=6 Dp10Yey=9	Unpaired t-test (two tailed)	t(13)=0.57	0.58	NA
Supp. Fig. 8l	WT=6 Dp17Yey=6	Unpaired t-test (two tailed)	t(10)=0.69	0.50	NA

733

Supplementary Figure 9					
	N	Test	Test value	p value	Post-hoc test
Supp. Fig. 9a	WT=11 Dp1Tyb=9	Mann-Whitney (two tailed)	U=26.0	0.08	NA
Supp. Fig. 9b	WT=6 Dp10Yey=9	Mann-Whitney (two tailed)	U=16.0	0.22	NA
Supp. Fig. 9c	WT=6 Dp17Yey=6	Mann-Whitney (two tailed)	U=9.0	0.18	NA
Supp. Fig. 9d	WT=11 Dp1Tyb=9	Mann-Whitney (two tailed)	U=44.0	0.69	NA
Supp. Fig. 9e	WT=6 Dp10Yey=9	Mann-Whitney (two tailed)	U=13.0	0.11	NA
Supp. Fig. 9f	WT=6 Dp17Yey=6	Mann-Whitney (two tailed)	U=12.0	0.39	NA

734

735 **Supplementary Table 3: Summary of Trial and Animal numbers for the Longitudinal Study**

	3 months						
	Dp1Tyb	WT	Dp10Yey	WT	Dp17Yey	WT	Mean
n	4	6	5	3	6	5	4.83
All Trials (Mean)	8.75	8.17	9.40	6.67	10.17	9.80	8.83
All Trials (SD)	1.89	2.48	0.89	3.51	0.41	0.45	1.61
Artefact Trials (Mean)	2.50	1.17	2.00	0.00	1.00	0.40	1.18
Artefact Trials (SD)	3.32	2.40	3.39	0.00	0.89	0.89	1.82
Included Trials (Mean)	6.25	7.00	7.40	6.67	9.17	9.40	7.65
Included Trials (SD)	2.87	2.61	4.22	3.51	0.98	0.89	2.51

	6 months						
	Dp1Tyb	WT	Dp10Yey	WT	Dp17Yey	WT	Mean
n	4	6	5	3	6	5	4.83
All Trials (Mean)	12.50	10.83	10.00	10.33	10.00	10.00	10.61
All Trials (SD)	4.36	1.17	0.00	0.58	0.00	0.00	1.02
Artefact Trials (Mean)	0.00	0.33	0.00	0.00	0.67	0.20	0.20
Artefact Trials (SD)	0.00	0.52	0.00	0.00	0.82	0.45	0.30
Included Trials (Mean)	12.50	10.50	10.00	10.33	9.33	9.80	10.41
Included Trials (SD)	4.36	1.52	0.00	0.58	0.82	0.45	1.29

	9 months						
	Dp1Tyb	WT	Dp10Yey	WT	Dp17Yey	WT	Mean
n	3	4	4	2	6	5	4
All Trials (Mean)	10.33	12.25	10.25	10.00	10.17	10.40	10.57
All Trials (SD)	0.58	5.19	2.06	0.00	0.41	0.55	1.46
Artefact Trials (Mean)	0.00	0.25	0.00	0.50	0.33	0.00	0.18
Artefact Trials (SD)	0.00	0.50	0.00	0.71	0.52	0.00	0.29
Included Trials (Mean)	10.33	12.00	10.25	9.50	9.83	10.40	10.39
Included Trials (SD)	0.58	4.69	2.06	0.71	0.75	0.55	1.56

736

References

1. de Graaf, G., Buckley, F. & Skotko, B. G. Estimates of the live births, natural losses, and elective terminations with Down syndrome in the United States. *Am. J. Med. Genet. A.* **167**, 756–767 (2015).

2. Hanney, M. *et al.* Memantine for dementia in adults older than 40 years with Down's syndrome (MEADOWS): a randomised, double-blind, placebo-controlled trial. *The Lancet* **379**, 528–536 (2012).

3. Sherman, S. L., Allen, E. G., Bean, L. H. & Freeman, S. B. Epidemiology of Down syndrome. *Ment. Retard. Dev. Disabil. Res. Rev.* **13**, 221–227 (2007).

4. Loane, M. *et al.* Twenty-year trends in the prevalence of Down syndrome and other trisomies in Europe: impact of maternal age and prenatal screening. *Eur. J. Hum. Genet.* **21**, 27 (2012).

5. Wu, J. & Morris, J. K. Trends in maternal age distribution and the live birth prevalence of Down's syndrome in England and Wales: 1938–2010. *Eur. J. Hum. Genet.* **21**, 1032–1033 (2013).

6. Lott, I. T. & Dierssen, M. Cognitive deficits and associated neurological complications in individuals with Down's syndrome. *Lancet Neurol.* **9**, 623–633 (2010).

7. Grieco, J., Pulsifer, M., Seligsohn, K., Skotko, B. & Schwartz, A. Down syndrome: Cognitive and behavioral functioning across the lifespan. *Am. J. Med. Genet. C Semin. Med. Genet.* **169**, 135–149 (2015).

8. Pennington, B. F., Moon, J., Edgin, J., Stedron, J. & Nadel, L. The Neuropsychology of Down Syndrome: Evidence for Hippocampal Dysfunction. *Child Dev.* **74**, 75–93 (2003).

9. Rowe, J., Lavender, A. & Turk, V. Cognitive executive function in Down's syndrome. *Br. J. Clin. Psychol.* **45**, 5–17 (2006).

10. Lanfranchi, S., Jerman, O., Dal Pont, E., Alberti, A. & Vianello, R. Executive function in adolescents with Down Syndrome. *J. Intellect. Disabil. Res.* **54**, 308–319 (2010).

11. Lavenex, P. B. *et al.* Allocentric spatial learning and memory deficits in Down syndrome. *Front. Psychol.* **6**, 62 (2015).

763   12. Clark Caron A.C., Fernandez Fabian, Sakhon Stella, Spanò Goffredina & Edgin Jamie O. The

764   medial temporal memory system in Down syndrome: Translating animal models of hippocampal

765   compromise. *Hippocampus* **27**, 683–691 (2017).

766   13. Nadel, L. Down's syndrome: a genetic disorder in biobehavioral perspective. *Genes Brain Behav.*

767   **2**, 156–166 (2003).

768   14. Nelson, L. *et al.* Learning and memory as a function of age in Down syndrome: A study using

769   animal-based tasks. *Progress in Neuro-Psychopharmacology and Biological Psychiatry* **29**, 443–

770   453 (2005).

771   15. Anderson, J. S. *et al.* Abnormal brain synchrony in Down Syndrome. *NeuroImage Clin.* **2**, 703–

772   715 (2013).

773   16. Ruiz-Mejias, M. *et al.* Overexpression of Dyrk1A, a Down Syndrome Candidate,

774   Decreases Excitability and Impairs Gamma Oscillations in the Prefrontal Cortex. *J. Neurosci.* **36**,

775   3648 (2016).

776   17. Duchon, A. & Herault, Y. DYRK1A, a Dosage-Sensitive Gene Involved in Neurodevelopmental

777   Disorders, Is a Target for Drug Development in Down Syndrome. *Front. Behav. Neurosci.* **10**, 104

778   (2016).

779   18. J. O'Keefe, L. N. *The Hippocampus as a Cognitive Map*. (Oxford University Press, 1978).

780   19. Bohbot, V. D., Copara, M. S., Gotman, J. & Ekstrom, A. D. Low-frequency theta oscillations in the

781   human hippocampus during real-world and virtual navigation. *Nat. Commun.* **8**, 14415 (2017).

782   20. Winson, J. Loss of hippocampal theta rhythm results in spatial memory deficit in the rat. *Science*

783   **201**, 160 (1978).

784   21. Guderian, S., Schott, B. H., Richardson-Klavehn, A. & Düzel, E. Medial temporal theta state

785   before an event predicts episodic encoding success in humans. *Proc. Natl. Acad. Sci.* **106**, 5365

786   (2009).

787   22. Fell, J. & Axmacher, N. The role of phase synchronization in memory processes. *Nat. Rev.*

788   *Neurosci.* **12**, 105 (2011).

789   23. Hasselmo, M. E., Bodelon, C. & Wyble, B. P. A proposed function for hippocampal theta rhythm:

790   separate phases of encoding and retrieval enhance reversal of prior learning. *Neural Comput.*

791   **14**, 793–817 (2002).

792   24. Buzsáki, G. & Chrobak, J. J. Temporal structure in spatially organized neuronal ensembles: a role

793   for interneuronal networks. *Curr. Opin. Neurobiol.* **5**, 504–510 (1995).

794   25. Canolty, R. T. *et al.* High Gamma Power Is Phase-Locked to Theta Oscillations in Human

795   Neocortex. *Science* **313**, 1626 (2006).

796   26. Sirota, A. *et al.* Entrainment of Neocortical Neurons and Gamma Oscillations by the

797   Hippocampal Theta Rhythm. *Neuron* **60**, 683–697 (2008).

798   27. Tort, A. B. L., Komorowski, R. W., Manns, J. R., Kopell, N. J. & Eichenbaum, H. Theta–gamma

799   coupling increases during the learning of item–context associations. *Proc. Natl. Acad. Sci.* **106**,

800   20942–20947 (2009).

801   28. Raghavachari, S. *et al.* Gating of Human Theta Oscillations by a Working Memory Task. *J.*

802   *Neurosci.* **21**, 3175 (2001).

803   29. Griesmayr, B., Gruber, W. R., Klimesch, W. & Sauseng, P. Human frontal midline theta and its

804   synchronization to gamma during a verbal delayed match to sample task. *Neurobiol. Learn.*

805   *Mem.* **93**, 208–215 (2010).

806   30. Klimesch, W. *et al.* Theta synchronization during episodic retrieval: neural correlates of

807   conscious awareness. *Cogn. Brain Res.* **12**, 33–38 (2001).

808   31. Kaplan, R. *et al.* Medial prefrontal theta phase coupling during spatial memory retrieval.

809   *Hippocampus* **24**, 656–665 (2014).

810   32. Jones, M. W. & Wilson, M. A. Theta Rhythms Coordinate Hippocampal–Prefrontal Interactions in

811   a Spatial Memory Task. *PLOS Biol.* **3**, e402 (2005).

812   33. Siapas, A. G., Lubenov, E. V. & Wilson, M. A. Prefrontal Phase Locking to Hippocampal Theta

813   Oscillations. *Neuron* **46**, 141–151 (2005).

814   34. Young, C. K. & McNaughton, N. Coupling of Theta Oscillations between Anterior and Posterior

815   Midline Cortex and with the Hippocampus in Freely Behaving Rats. *Cereb. Cortex* **19**, 24–40

816   (2009).

817   35. Benchenane, K. *et al.* Coherent Theta Oscillations and Reorganization of Spike Timing in the

818   Hippocampal- Prefrontal Network upon Learning. *Neuron* **66**, 921–936 (2010).

819   36. Guitart-Masip, M. *et al.* Synchronization of Medial Temporal Lobe and Prefrontal Rhythms in

820   Human Decision Making. *J. Neurosci.* **33**, 442 (2013).

821   37. Lana-Elola, E. *et al.* Genetic dissection of Down syndrome-associated congenital heart defects

822   using a new mouse mapping panel. *eLife* **5**, e11614 (2016).

823   38. Yu, T. *et al.* A mouse model of Down syndrome trisomic for all human chromosome 21 syntenic

824   regions. *Hum. Mol. Genet.* **19**, 2780–2791 (2010).

825   39. Deacon, R. M. J. & Rawlins, J. N. P. T-maze alternation in the rodent. *Nat Protoc.* **1**, 7–12 (2006).

826   40. Wenk, G. L. Assessment of spatial memory using the T maze. *Curr. Protoc. Neurosci.* **Chapter 8**,

827   Unit 8.5B (2001).

828   41. Sarnyai, Z. *et al.* Impaired hippocampal-dependent learning and functional abnormalities in the

829   hippocampus in mice lacking serotonin$_{1A}$ receptors. *Proc. Natl. Acad. Sci.* **97**, 14731 (2000).

830   42. Shoji, H., Hagihara, H., Takao, K., Hattori, S. & Miyakawa, T. T-maze Forced Alternation and Left-

831   right Discrimination Tasks for Assessing Working and Reference Memory in Mice. *J. Vis. Exp.*

832   *JoVE* 3300 (2012). doi:10.3791/3300

833   43. Bizon, J. L., Foster, T. C., Alexander, G. E. & Glisky, E. L. Characterizing cognitive aging of working

834   memory and executive function in animal models. *Front. Aging Neurosci.* **4**, 19 (2012).

835   44. Sherman, B. L. *et al.* The use of a T-maze to measure cognitive-motor function in cats (Felis

836   catus). *J. Vet. Behav. Clin. Appl. Res. Off. J. Aust. Vet. Behav. Interest Group Int. Work. Dog Breed.*

837   *Assoc.* **8**, 32–39 (2013).

838   45. Pioli, E. Y. *et al.* An automated maze task for assessing hippocampus-sensitive memory in mice().

839   *Behav. Brain Res.* **261**, 249–257 (2014).

840   46. Arron, J. R. *et al.* NFAT dysregulation by increased dosage of DSCR1 and DYRK1A on

841   chromosome 21. *Nature* **441**, 595 (2006).

842   47. Guimera, J., Casas, C., Estivill, X. & Pritchard, M. HumanMinibrainHomologue (MNBH/DYRK1):

843   Characterization, Alternative Splicing, Differential Tissue Expression, and Overexpression in

844   Down Syndrome. *Genomics* **57**, 407–418 (1999).

845   48. Park, J., Song, W.-J. & Chung, K. C. Function and regulation of Dyrk1A: towards understanding

846   Down syndrome. *Cell. Mol. Life Sci.* **66**, 3235–3240 (2009).

847   49. Fotaki, V. *et al.* Dyrk1A Haploinsufficiency Affects Viability and Causes Developmental Delay and

848   Abnormal Brain Morphology in Mice. *Mol. Cell. Biol.* **22**, 6636–6647 (2002).

849   50. Tejedor Francisco J. & Hämmerle Barbara. MNB/DYRK1A as a multiple regulator of neuronal

850   development. *FEBS J.* **278**, 223–235 (2010).

851   51. Hämmerle Barbara, Elizalde Carina & Tejedor Francisco J. The spatio-temporal and subcellular

852   expression of the candidate Down syndrome gene Mnb/Dyrk1A in the developing mouse brain

853   suggests distinct sequential roles in neuronal development. *Eur. J. Neurosci.* **27**, 1061–1074

854   (2008).

855   52. Souchet, B. *et al.* Excitation/inhibition balance and learning are modified by Dyrk1a gene

856   dosage. *Neurobiol. Dis.* **69**, 65–75 (2014).

857   53. Richard Gregory R. *et al.* Speed modulation of hippocampal theta frequency correlates with

858   spatial memory performance. *Hippocampus* **23**, 1269–1279 (2013).

859   54. Colgin, L. L. *et al.* Frequency of gamma oscillations routes flow of information in the

860   hippocampus. *Nature* **462**, 353 (2009).

861   55. Bragin, A. *et al.* Gamma (40-100 Hz) oscillation in the hippocampus of the behaving rat. *J.

862   Neurosci.* **15**, 47 (1995).

863   56. Lisman, J. The theta/gamma discrete phase code occuring during the hippocampal phase

864   precession may be a more general brain coding scheme. *Hippocampus* **15**, 913–922 (2005).

865 57. Benchenane, K., Tiesinga, P. H. & Battaglia, F. P. Oscillations in the prefrontal cortex: a gateway

866   to memory and attention. *Behav. Cogn. Neurosci.* **21**, 475–485 (2011).

867 58. Vega, J. N., Hohman, T. J., Pryweller, J. R., Dykens, E. M. & Thornton-Wells, T. A. Resting-State

868   Functional Connectivity in Individuals with Down Syndrome and Williams Syndrome Compared

869   with Typically Developing Controls. *Brain Connect.* **5**, 461–475 (2015).

870 59. Foster, H.L, Small, J.D & Fox, J.G. *The Mouse in Biomedical Research*. (Elsevier, 2007).

871 60. Lalonde, R. The neurobiological basis of spontaneous alternation. *Neurosci. Biobehav. Rev.* **26**,

872   91–104 (2002).

873 61. Jakobsen, L. H., Sorensen, J. M., Rask, I. K., Jensen, B. S. & Kondrup, J. Validation of reaction time

874   as a measure of cognitive function and quality of life in healthy subjects and patients. *Nutrition*

875   **27**, 561–570 (2011).

876 62. Yu, T. *et al.* Effects of individual segmental trisomies of human chromosome 21 syntenic regions

877   on hippocampal long-term potentiation and cognitive behaviors in mice. *Brain Res.* **1366**, 162–

878   171 (2010).

879 63. Belichenko, P. V. *et al.* Down Syndrome Cognitive Phenotypes Modeled in Mice Trisomic for All

880   HSA 21 Homologues. *PLOS ONE* **10**, e0134861 (2015).

881 64. Aziz, N. M. *et al.* Lifespan analysis of brain development, gene expression and behavioral

882   phenotypes in the Ts1Cje, Ts65Dn and Dp(16)1/Yey mouse models of Down syndrome. *Dis.*

883   *Models Amp Mech.* (2018). doi:10.1242/dmm.031013

884 65. Levenga, J., Peterson, D. J., Cain, P. & Hoeffer, C. A. Sleep Behavior and EEG Oscillations in Aged

885   Dp(16)1Yey/+ Mice: A Down Syndrome Model. *Neuroscience* **376**, 117–126 (2018).

886 66. Reisel, D. *et al.* Spatial memory dissociations in mice lacking GluR1. *Nat. Neurosci.* **5**, 868 (2002).

887 67. Sanderson, D. J. & Bannerman, D. M. The role of habituation in hippocampus-dependent spatial

888   working memory tasks: Evidence from GluA1 AMPA receptor subunit knockout mice.

889   *Hippocampus* **22**, 981–994 (2012).

890   68. D'Hooge, R. & De Deyn, P. P. Applications of the Morris water maze in the study of learning and

891   memory. *Brain Res. Rev.* **36**, 60–90 (2001).

892   69. Tort, A. B. L. *et al.* Dynamic cross-frequency couplings of local field potential oscillations in rat

893   striatum and hippocampus during performance of a T-maze task. *Proc. Natl. Acad. Sci.* **105**,

894   20517–20522 (2008).

895   70. Tort, A. B. L., Komorowski, R., Eichenbaum, H. & Kopell, N. Measuring Phase-Amplitude Coupling

896   Between Neuronal Oscillations of Different Frequencies. *J. Neurophysiol.* **104**, 1195–1210

897   (2010).

898   71. Jensen, O. & Lisman, J. E. Hippocampal sequence-encoding driven by a cortical multi-item

899   working memory buffer. *Trends Neurosci.* **28**, 67–72 (2005).

900   72. Poch, C., Fuentemilla, L., Barnes, G. R. & Düzel, E. Hippocampal Theta-Phase Modulation of

901   Replay Correlates with Configural-Relational Short-Term Memory Performance. *J. Neurosci.* **31**,

902   7038 (2011).

903   73. Lisman, J. & Idiart, M. Storage of 7 +/- 2 short-term memories in oscillatory subcycles. *Science*

904   **267**, 1512 (1995).

905   74. Leszczyński, M., Fell, J. & Axmacher, N. Rhythmic Working Memory Activation in the Human

906   Hippocampus. *Cell Rep.* **13**, 1272–1282 (2015).

907   75. Maris, E., van Vugt, M. & Kahana, M. Spatially distributed patterns of oscillatory coupling

908   between high-frequency amplitudes and low-frequency phases in human iEEG. *NeuroImage* **54**,

909   836–850 (2011).

910   76. Gupta, M., Dhanasekaran, A. R. & Gardiner, K. J. Mouse models of Down syndrome: gene

911   content and consequences. *Mamm. Genome* **27**, 538–555 (2016).

912   77. Block, A., Ahmed, M. M., Dhanasekaran, A. R., Tong, S. & Gardiner, K. J. Sex differences in

913   protein expression in the mouse brain and their perturbations in a model of Down syndrome.

914   *Biol. Sex Differ.* **6**, 24 (2015).

915 78. Inui, N., Yamanishi, M. & Tada, S. Simple Reaction Times and Timing of Serial Reactions of

916 Adolescents with Mental Retardation, Autism, and down Syndrome. *Percept. Mot. Skills* **81**,

917 739–745 (1995).

918 79. Vicari, S., Bellucci, S. & Carlesimo, G. A. Implicit and explicit memory: a functional dissociation in

919 persons with Down syndrome. *Neuropsychologia* **38**, 240–251 (2000).

920 80. Brunamonti, E. *et al.* Cognitive control of movement in down syndrome. *Res. Dev. Disabil.* **32**,

921 1792–1797 (2011).

922 81. Costanzo, F. *et al.* Executive functions in intellectual disabilities: A comparison between Williams

923 syndrome and Down syndrome. *Res. Dev. Disabil.* **34**, 1770–1780 (2013).

924 82. Jeewajee, A., Barry, C., O'Keefe, J. & Burgess, N. Grid cells and theta as oscillatory interference:

925 Electrophysiological data from freely moving rats. *Hippocampus* **18**, 1175–1185 (2008).

926 83. Thierry, A.-M., Gioanni, Y., Dégénétais, E. & Glowinski, J. Hippocampo-prefrontal cortex

927 pathway: Anatomical and electrophysiological characteristics. *Hippocampus* **10**, 411–419 (2000).

928 84. Varela, C., Kumar, S., Yang, J. Y. & Wilson, M. A. Anatomical substrates for direct interactions

929 between hippocampus, medial prefrontal cortex, and the thalamic nucleus reuniens. *Brain*

930 *Struct. Funct.* **219**, 911–929 (2014).

931 85. Zhong, Y.-M., Yukie, M. & Rockland, K. S. Distinctive morphology of hippocampal CA1

932 terminations in orbital and medial frontal cortex in macaque monkeys. *Exp. Brain Res.* **169**, 549–

933 553 (2006).

934 86. Colgin, L. L. Oscillations and hippocampal–prefrontal synchrony. *Behav. Cogn. Neurosci.* **21**, 467–

935 474 (2011)

936 87. Neumann, F. *et al.* DYRK1A inhibition and cognitive rescue in a Down syndrome mouse model

937 are induced by new fluoro-DANDY derivatives. *Sci. Rep.* **8**, 2859 (2018).

938 88. Chang, P., Hashemi, K. S. & Walker, M. C. A novel telemetry system for recording EEG in small

939 animals. *J. Neurosci. Methods* **201**, 106–115 (2011).

940 89. Paxinos, G, F., K. *The Mouse Brain in Stereotaxic Coordinates*. (Academic Press, 2012).

941   90. Spellman, T. *et al.* Hippocampal-prefrontal input supports spatial encoding in working memory.

942   *Nature* **522**, 309–314 (2015).

943   91. Chang, P., Fabrizi, L., Olhede, S. & Fitzgerald, M. The Development of Nociceptive Network

944   Activity in the Somatosensory Cortex of Freely Moving Rat Pups. *Cereb. Cortex* **26**, 4513–4523

945   (2016).

946   92. De Chaumont, F. et al. Icy: an open bioimage informatics platform for extended reproducible

947   research. *Nature Methods* **9**, 690-696 (2012)

948   93.   Berens, P. CircStat: A MATLAB Toolbox for Circular Statistics. *J. Stat. Softw. Vol 1 Issue 10*
949   *2009* (2009).